CHAPTER 3
LABORATORY TESTING PROGRAM

3.1 Description of Laboratory Testing Program

Review of the literature indicates that there is very little published information on stress-strain properties of soil-bentonite mixtures. Consequently, a laboratory testing program with the following objectives was completed: 1) to add to the body of knowledge on stress-strain properties of soil-bentonite mixtures and 2) to provide information useful for choosing an appropriate constitutive model for soil-bentonite. The test procedures and results are presented in this chapter. Interpretation of the tests to evaluate constitutive models is presented in Chapter 4.

Three soil-bentonite mixtures were fabricated for the laboratory testing program. They are referred to as SB1, SB2, and SB3. SB1 and SB2 are identical except that SB1 was made with distilled water and SB2 was made with tap water. SB2 was created for hydraulic conductivity tests since tap water is recommended over distilled water for hydraulic conductivity testing (Daniel 1994). SB3 was also made with tap water. An extensive lab testing program was performed on SB1 to fully characterize its material properties. The following tests were run on SB1: index tests, slump tests, hydraulic conductivity tests, 1-D consolidation tests, isotropic consolidation tests, a K_o consolidation test, and CU and CD triaxial compression tests. Only hydraulic conductivity tests were run on SB2. The following tests were run on SB3: index tests, hydraulic conductivity tests, 1-D consolidation tests, and CU and CD triaxial compression tests. The laboratory tests were run with the assistance of Gerry Heslin and Laura Henry, who were graduate research assistants at Virginia Tech at the time.

3.2 Grain Size Distribution and Index Tests

Based on several references in the literature (D'Appolonia 1980; Millet et al. 1992; Evans 1991; Spooner et al. 1985), a typical soil-bentonite should have the following characteristics: well-graded granular matrix with 30% to 40% fines, permeability of less than 10^{-7} cm/sec, 1% to 3 % bentonite by weight, and 4 to 6 inch slump. The gradation of soil-bentonite mixture SB1 was designed to represent a soil-bentonite with the recommended properties. SB1 is a well-graded sand with 34% plastic fines and 1.5% bentonite. SB2 has the same gradation as SB1. The gradation of soil-bentonite mixture SB3 was designed with a different gradation than SB1, but one that may still occur in the field. SB3 is medium to fine sand with 16% non-plastic fines and 3% bentonite. The following soils were blended in various percentages to fabricate SB1, SB2, and SB3, with their classification according to the Unified Soil Classification System (USCS) given in parentheses:

1. Grottoes concrete sand (SP): clean, poorly graded, coarse to fine natural sand with subangular particles from a quarry in Grottoes, Virginia.
2. Yatesville silty sand (SM): alluvial silty fine sand with 47% non-plastic fines from Yatesville lake dam in Lawrence County, Kentucky (Filz 1992)
3. Blacksburg clay (CH): residual, highly plastic clay with 10% silt from Blacksburg, Virginia.
4. Light Castle sand (SP): clean, uniform fine sand with subangular quartz particles from a quarry in Craig County, Virginia (Filz 1992).
5. Bentonite: sodium montmorillinite sold commercially under the name Hydrogel 90 by Wyo-Ben, Inc.

SB1 and SB2 consist of approximately 50% Grottoes concrete sand (by dry weight), 39% Yatesville silty sand, 10% Blacksburg clay, and 1.5% bentonite. SB3 consists of approximately 68% Light Castle sand, 29% Yatesville silty sand, and 3% bentonite. The soil-bentonite was made by blending the soils dry (without the bentonite), and then adding

the bentonite in slurry form. For SB1, the bentonite was mixed with distilled water and allowed to hydrate 24 hours to create the slurry. For SB2 and SB3, the bentonite was hydrated for 24 hours with tap water instead of distilled water to create the slurry.

The grain size distributions of SB1, SB2, and SB3 are plotted in Figure 3.1. The maximum grain size was limited to particles passing the No. 4 sieve, 0.187 inches (4.75 mm).

Index properties of the soil-bentonite mixtures are shown in Table 3.1. SB1 classifies as a clayey sand (SC) according to the USCS. SB3 classifies as a silty sand (SM). SB1 contains 35% fines, and SB3 contains 16% fines (portion passing the No. 200 sieve).

Atterberg Limits tests were run on the portion of the soil-bentonite mixtures passing the No. 40 sieve as specified by ASTM D-4318. The Atterberg Limits indicate that the portion of SB1 passing the No. 40 sieve falls above the A-line on the plasticity chart. The portion of SB3 passing the No. 40 sieve is non-plastic.

Table 3.1 Index Properties of Soil-Bentonite Mixtures SB1 and SB3

Soil-Bentonite Mixture	% Bentonite	USCS Classification	G_s	% Sand	% Fines	LL	PI
SB1	1.5	SC	2.71	35	35	34	18
SB3	3.0	SM	2.65	16	16	NP	NP

The relationship between slump and water content for SB1 is shown in Figure 3.2 by the closed circles. As the water content increases from 25% to 35%, the slump for SB1 increases from approximately zero inches to approximately 6 inches. Data from four other soil-bentonite mixtures from D'Appolonia (1980) are also shown in the figure. The water content versus slump relationship is very similar for all the different soil-bentonite mixtures. For consolidation tests and triaxial tests, the water content of the soil-bentonite was

adjusted to achieve a slump of 4-6 inches. This is the range of slump recommended for placement of soil-bentonite in the field (Evans 1991; Millet et al 1992).

3.3 Hydraulic Conductivity Tests

Hydraulic conductivity tests were conducted on soil-bentonite mixtures SB1, SB2, and SB3. The tests were performed using compaction mold permeameters, consolidometer permeameters, the API filter press, and flexible-wall permeameters. The results of all the tests are shown in Figure 3.3. Data from the literature are also plotted in the figure, and are discussed below.

Experimental Procedures

Three hydraulic conductivity tests were run on SB1 in compaction mold permeameters. The soil-bentonite was spooned into the mold and rodded to eliminate air voids. The samples were 4 inches in diameter and the final height was approximately 4 inches. Surcharge weights were applied to consolidate the soil-bentonite to various effective stresses. The average vertical effective stress in the sample versus the hydraulic conductivity is shown in Figure 3.3. The two tests at lower pressure were permeated downward in falling head tests. In order to achieve the higher pressures for the third test, considerable weights were stacked above the top of the compaction mold. The top was left unassembled and a falling head test was run by permeating upward.

As part of a related research project at Virginia Tech (Heslin et al. 1997), hydraulic conductivity tests were run on SB2 and SB3 using flexible-wall permeameters, consolidometer permeameters, and the API filter press. The following tests were run on SB2: One flexible-wall permeability test, two consolidation permeameter tests, and two API filter press tests. Two consolidation permeameter tests and three API filter press tests were run on SB3. For each test, the hydraulic conductivity was found at three to seven different pressures.

The flexible-wall test was run using the falling headwater - rising tailwater method described in ASTM D-5048 without backpressure. Samples were 2.8 inches in diameter and 3.3 inches in height prior to testing. A forming jacket was used to support the sample before application of the cell pressure. The forming jacket was left in place during the test. The effective isotropic consolidation pressure is plotted versus the hydraulic conductivity in Figure 3.3.

Standard incremental load tests were run in the consolidometer permeameter without backpressure, as described below in Section 3.4. Samples were 2.5 inches in diameter and 1 inch in height. Falling head test hydraulic conductivity tests were conducted after the end of primary consolidation. The vertical effective consolidation pressure is plotted versus the hydraulic conductivity in Figure 3.3.

The API filter press is an apparatus commonly used to measure the filtrate loss of slurry. It has also been used to measure the hydraulic conductivity of soil-bentonite during soil-bentonite mix design and for QA/QC (Barvenik and Ayers 1987). The API filter press is a rigid wall cell 3 inches in diameter. Air pressure is applied to the top of the specimen. A more detailed description of the equipment and test procedure for the consolidometer permeameter and API filter press test is given in Heslin et al. (1997). A surcharge was used inside the API cell since it was found that hydraulic fracture occurs in tests without surcharge. In some of the API filter press tests at the higher pressures, it is believed that problems occurred with either migration of fines or washing of fines out of the specimen. These hydraulic conductivity measurements are not included in Figure 3.3.

As described in Heslin et al. (1997), running a hydraulic conductivity test in the API filter press results in a soil-bentonite specimen that has zero vertical effective stress at the top of the specimen and a maximum value of vertical effective stress at the bottom of the speci-

men. In order to properly interpret the results, the method described by Heslin et al. (1997) was used to estimate the apparent pressure that should be associated with the measured gross hydraulic conductivity. This method uses the seepage consolidation theory by Fox and Baxter (1997), and applies the theory to analysis of hydraulic conductivity tests in the API filter press. For all of the API tests, the apparent pressure is plotted versus the gross hydraulic conductivity in Figure 3.3.

Results

The results in Figure 3.3 show that the four different permeameter types all give similar results. Especially consistent results were found for the consolidometer permeameter, flexible-wall permeameter, and API test. Less consistent results were found for the compaction mold permeameter.

Essentially the same hydraulic conductivity was measured for SB1 and SB2. The soil-bentonite mixtures SB1 and SB2 are identical except that SB1 was created and permeated with distilled water and SB2 was created and permeated with tap water. SB2 was created because distilled water is not recommended for permeability testing (Daniel 1994; Dunn and Mitchell 1984). The results show that for this soil-bentonite mixture, the effect of using distilled water versus tap water for hydraulic conductivity testing is not significant.

For all of the soil-bentonite mixtures, the hydraulic conductivity decreases with increasing vertical consolidation pressure. The hydraulic conductivity for SB2 decreases from approximately $1x10^{-7}$ cm/sec at 100 psf to $5x10^{-8}$ cm/sec at 1000 psf. The hydraulic conductivity for SB3 decreases only slightly with increases in consolidation pressure. The hydraulic conductivity for SB3 is approximately $5x10^{-8}$ cm/sec at 100 psf and $3x10^{-8}$ cm/sec at 1500 psf. SB3 has a lower hydraulic conductivity than SB2 at all consolidation pressures. The percentage of bentonite appears to have a larger influence on hydraulic conductivity than fines content since SB3 has 16% non-plastic fines and 3% bentonite and

SB1 has 35% plastic fines and 1% bentonite. SB2 and SB3 both have hydraulic conductivity values in the range of typically desired soil-bentonite mixtures.

Also plotted in Figure 3.3 is data from *Barrier* (1995) that was obtained from several other soil-bentonite mixtures. The data from *Barrier* (1995) includes results from McCandless and Bodocsi (1988) and Day (unpublished). As discussed previously in Section 2.4, the horizontal hydraulic conductivity data from McCandless and Bodocsi (1988) was measured under a combined vertical surcharge and horizontal hydraulic pressure. It appears that this data was misinterpreted in *Barrier* (1995) and is therefore not included in Figure 3.3. The hydraulic conductivity values of SB2 and SB3 appear to be in the same range and show similar trends as the *Barrier* data from Day, although the data from Day exhibits a greater sensitivity to vertical consolidation pressure.

3.4 Consolidation Tests

Two 1-D consolidation tests and two isotropic consolidation tests were performed on SB1. Two 1-D consolidation tests were performed on SB3.

The two 1-D consolidation tests on SB1 (C5 and C6) were standard incremental load tests performed in accordance with ASTM D-2435. The samples were 2.5 inches in diameter and 1 inch in height. The soil-bentonite was spooned into the consolidation ring and rodded to eliminate large air voids. Loads were added through a dead weight hanger system using a load increment ratio of 1 (doubling of the load), and a load increment duration of 24 hours. Back pressure was not used. The data was corrected for machine deflection that was estimated using a steel sample. In order to obtain the appropriate machine deflection curve, it was found that the filter paper needed considerable time to consolidate under each load (approximately 4 hours). The void ratio versus vertical effective stress for the two tests are plotted in Figure 3.4 and Figure 3.5. The coefficient of consolidation, C_v, was calculated for primary loading using the Casagrande method and

the Taylor method. The values of C_v are plotted versus the average pressure for each stress increment.

A trend in the time deformation data for SB1 can be seen from Figures 3.4 and 3.5. As the effective stress increases, the value of the coefficient of consolidation, C_v, increases considerably. C_v is defined in equation 3.1, and increases from approximately 5 ft^2/yr at 100 psf to 80 ft^2/yr at 10,000 psf. C_v is a function of the compressibility and permeability of the soil-bentonite, which are both decreasing as the effective stress increases. Therefore, it appears that the compressibility is decreasing at a faster rate than the permeability.

$$C_v = \frac{k(1+e_o)}{a_v \gamma_w} \tag{3.1}$$

where: k = hydraulic conductivity

e_o = initial void ratio

γ_w = unit weight of water

a_v = coefficient of compressibility

The C_v values for SB1 can be compared to typical values for clays. Correlations of C_v with liquid limit (Holtz and Kovacs 1981) indicate that a typical remolded clay with the same liquid limit as SB1 (LL=34), would have a C_v value less than or equal to 32 ft^2/yr. Three soil-bentonite mixtures presented by Khoury et al. (1992) had C_v values ranging from 70 to 292 ft^2/yr for the stress range of 2000-4000 psf. For this stress range, SB1 has a C_v of approximately 40 ft^2/yr. The coefficient of consolidation for SB1 is slightly higher than for a clay with similar liquid limit, but significantly less than the values for soil-bentonite mixtures reported by Khoury et al. (1992).

Two isotropic consolidation tests on SB1 (IC-1 and IC-2) were conducted in a triaxial cell on 2.8 inch diameter samples. The initial height of the samples was approximately 5.6 inches. Special procedures that were developed for triaxial compression testing of soil-

bentonite were also used to prepare the isotropic consolidation tests. The soil-bentonite was spooned into a forming jacket and rodded to eliminate large air voids. The samples were consolidated inside the forming jacket to an initial pressure of at least 3 psi. It was found that a 3 psi consolidation pressure was required for the soil-bentonite to be able to maintain its shape without the forming jacket. After the sample was fully consolidated to the initial pressure, the triaxial cell was disassembled and the forming jacket was removed. The sample dimensions were measured at this time. The cell was then reassembled and the sample was backpressure saturated in small increments in order to avoid overconsolidating the sample. A B-value of 0.99 was reached. Next, the sample was consolidated to a final pressure to eliminate disturbance effects from the process of removing the forming jacket.

The sample used for isotropic consolidation test IC_1 was initially consolidated to 3 psi and finally consolidated to 5 psi. The sample was then loaded using a load increment ratio of 2/3 and a load increment duration of approximately 48 hours. The sample for isotropic consolidation test IC_2 was initially consolidated to 10 psi and finally consolidated to 20.3 psi. It was then unloaded to 10 psi and reloaded in increments of 2 psi in order to find the isotropic yield point. The void ratio versus vertical effective stress curves for IC_1 and IC_2 are shown in Figure 3.6 and Figure 3.7.

Two 1-D consolidation tests were conducted on specimens of SB3 (CP5 and CP6) in the consolidometer permeameter cells described in Section 3.3 of this report. The void ratio versus vertical effective stress curves for the two tests are shown in Figure 3.8 and Figure 3.9. Falling head hydraulic conductivity tests were run at various consolidation pressures in these tests. The results of the hydraulic conductivity tests are described in Section 3.3.

The results of all the consolidation tests are summarized in Table 3.2. Values of the compression index C_c and the compression ratio are listed. The compression ratio was

calculated for the stress increment between 1000 psf and 4000 psf. The void ratio, e, at 1000 psf was used to calculate the compression ratio. Values of the recompression index, C_r, are listed together with the preconsolidation pressures, σ_p', at the time of rebound.

Holtz and Kovacs (1981) report that the range of compression index for a typical normally consolidated medium-sensitive clay is 0.2 to 0.5. The average 1-D compression index for SB1 is 0.19, which is just outside the lower bound of this range. The average isotropic compression index for SB1 is 0.15, which is also below this range. The average compression index for SB3 is 0.088, which is approximately 2 times smaller than the value for SB1. It seems reasonable that SB1 and SB3 are less compressible than a medium sensitive clay since SB1 is a clayey sand (SC) and SB3 is a silty sand (SM).

Table 3.2 Consolidation Test Results on SB1 and SB3

Test Number	Soil-Bentonite Mixture	Test Type	Initial w%	e at 1000 psf	C_c	Compression Ratio	C_r at σ_p' (psf)
C5	SB1	1-D	30.3	0.631	0.18	0.11	0.010 at 4200 psf
C6	SB1	1-D	31.7	0.614	0.20	0.12	0.0074 at 1100 psf 0.0095 at 8400 psf
IC_1	SB1	isotropic	23.5	0.560	0.16	0.10	0.011 at 5600 psf
IC_2	SB1	isotropic	31.9	NA	0.14	NA	0.013 at 2900 psf
CP5	SB3	1-D	28.9	0.594	0.082	0.051	0.0029 at 1600 psf
CP6	SB3	1-D	28.9	0.595	0.094	0.059	0.0027 at 1600 psf

Notes: The compression ratio was calculated for the stress increment between 1000 psf and 4000 psf.
The void ratio at 1000 psf was used to calculate the compression ratio.

The 1-D and isotropic compression ratios for SB1 are both about 0.11. The compression ratios were evaluated at the same stress increment as the data shown in Figure 2.2 (from D'Appolonia 1980) in order to compare them. The compression ratios for SB1 are approximately 1.7 times greater than the compression ratios reported by D'Appolonia for soil-bentonite mixtures with 35% plastic fines. However, the compression ratios for SB1 are in reasonable agreement with those of Khoury et al. (1992) shown in Table 2.1 and

Evans and Cooley (1993) shown in Table 2.2. The average compression ratio for SB3 is 0.056. This value is approximately 2.7 times greater than that reported data by D'Appolonia for soil-bentonite mixes with 16% non-plastic fines, and it is smaller than the values in Tables 2.1 and 2.2.

The void ratio versus major effective principal stress from the 1-D consolidation tests and the isotropic consolidations test for SB1 and SB3 are plotted together in Figure 3.10. The void ratios from the rebound and recompression stages are not shown. For SB1, the void ratios for the two 1-D consolidated tests (open circles) are consistently higher than the void ratios for two isotropically consolidated tests (open triangles). To verify the isotropic consolidation data, the void ratios from the end of the isotropic consolidation phase of CU triaxial tests are also plotted in the figure as open triangles. The isotropically consolidated triaxial tests give results consistent with the isotropic consolidation tests. For SB3, the void ratios from the two 1-D consolidation tests (black circles) lie slightly above the data from the three isotropically consolidated triaxial tests (black triangles). The data from the triaxial tests appear to have a slightly different slope than the one-dimensionally consolidated tests for SB3. The figure also shows that SB3 is less compressible than SB1.

The void ratios from the consolidation tests are plotted versus the mean effective stress in Figure 3.11. The mean effective stress was estimated for the 1-D consolidation tests using a K_o value of 0.57 for SB1 and a K_o value of 0.5 for SB3. The value of K_o for SB1 was measured in a K_o consolidation test, Ko_2, which is described later in this section. The K_o value for SB3 was assumed. For SB1, the void ratio appears to have the same relationship with the log of mean effective stress for both the 1-D and the isotropic consolidation tests. This holds for SB3 as well. Comparing Figures 3.10 and 3.11, the void ratio for a given soil-bentonite mixture appears to be a function of the mean effective stress rather than the vertical effective stress

3.5 Triaxial Tests

The following triaxial tests were run on SB1: Seven isotropically consolidated undrained triaxial compression tests (CU), one K_o consolidated undrained triaxial compression test, and nine isotropically consolidated drained triaxial compression tests (CD). The following triaxial tests were run on SB3: three CU tests, and two CD tests.

Experimental Procedures

2.8 inch diameter triaxial samples, formed with the largest triaxial equipment that was readily available, were used for testing the soil-bentonite. ASTM D4767 for CU tests recommends the sample diameter should be at least 6 times greater than the largest particle size. With the 2.8 inch diameter sample, the largest recommended particle size is approximately 0.5 inch. The maximum grain size for SB1 and SB3 was limited to passing the No. 4 sieve (0.2 inches), so the particle size criterion was satisfied. The initial height of the samples was approximately 5.6 inches.

Due to the soft nature of the soil-bentonite, a new method for forming the sample was developed. As previously described for the isotropic consolidation tests, samples were formed inside the triaxial cell in a forming mold (membrane expander). This method was chosen over consolidation in a batch consolidometer, which would have required higher pressures in order to extrude and trim the samples. The forming mold provided the least disturbance and allowed the samples to be formed at the lowest pressures. The samples were isotropically consolidated inside the forming mold to a pressure of 3 psi or greater. It was found that 3 psi isotropic pressure for this initial consolidation phase was necessary for the sample to maintain its shape. A special top cap was machined to slide inside the forming mold as the sample consolidated. No back pressure was used during the initial consolidation. The volume of water expelled was measured with a graduated cylinder. After the sample reached the end of primary consolidation at the initial pressure, the cell was disassembled. Drainage from the sample was prevented during cell disassembly. The

forming mold was removed and the sample dimensions were measured. The cell was then reassembled without the mold and the sample was backpressure saturated. After a B value above 0.97 was reached, the sample was consolidated to its final consolidation pressure. The final consolidation pressure was at least 1.5 times the initial consolidation pressure in order to minimize disturbance effects from the disassembly process.

After the final consolidation phase, the sample was sheared undrained (CU test) or drained (CD test). The samples were loaded at a constant strain rate. It is recommended that for CU tests, the time to failure should be five times t_{50} for pore pressure equalization throughout the sample (Brandon 1995), where t_{50}=time to 50% consolidation from the consolidation stage. For CD tests, time to failure should be 15 to 20 times t_{50} for pore pressure dissipation (Brandon 1995). For CU tests, it was decided to use a time to failure between five to seven times t_{50}. The strain to failure was estimated at 10% axial strain. Strain rates were typically $2x10^{-4}$ to $3x10^{-4}$ inch/min or $3x10^{-3}$ to $6x10^{-3}$ %/min. For CD tests, 15 to 20 times t_{50} was used for time to failure. The strain at failure was estimated as 15%. Strain rates were typically $1x10^{-4}$ to $2x10^{-4}$ inch/min or $2x10^{-3}$ to $3x10^{-3}$ %/min. Data acquisition was used to measure the load, effective stress or volume change, and axial deformation. The data acquisition was always verified with data taken by hand.

Area and Membrane Corrections

Several corrections were made to the data, which are described in more detail in Appendix A. An area correction was applied, which assumes that the sample deforms as a right circular cylinder. This correction is recommended by La Rochelle et al. (1988) for specimens exhibiting a bulging type failure, which occurred for all of the triaxial tests performed on soil-bentonite mixtures. After reviewing the literature on membrane corrections, a new membrane correction procedure was developed. The membrane corrections were based on the compression shell theory by Henkel and Gilbert (1952) with aspects of other membrane corrections in the literature (Duncan and Seed 1967; La Rochelle et al.

1988). The theory was extended to correct for the axial and radial stress on the sample during the consolidation phase. The correction during the consolidation phase was important for soil-bentonite testing due to the large strains that occurred during the consolidation phase. This correction resulted in a very slight anisotropic stress state at the end of the supposedly isotropic consolidation phase. The major effective stress after consolidation was in the radial direction. The difference in the major and minor effective principal stresses was 0.2 psi for low consolidation pressures (5 psi) and 0.8 psi for the largest consolidation pressure (39 psi). During the shearing phase, the membrane correction described in ASTM D4767 was applied to the axial stress. The modulus of the membrane used in the membrane corrections was the initial tangent modulus, which was measured experimentally. Piston friction in the triaxial cell was assumed to be constant and was zeroed out at the start of the test.

Isotropically Consolidated Undrained Triaxial Tests

Seven isotropically consolidated undrained triaxial tests (CU) were run on SB1 (CU_3 through CU_9). Two of the samples were used for isotropic consolidation tests before being sheared. Isotropic consolidation test IC_1 was sheared as CU_8 and IC_2 was sheared as CU_9. All of the samples were sheared essentially normally consolidated except for CU_8, which was sheared slightly overconsolidated. The data from the first two tests CU_1 and CU_2 was not of good quality and was not used. Several problems with data acquisition were solved and procedures were refined during the first two tests.

During undrained tests, it was found that pore pressures would build up in the sample after primary consolidation was complete and the drainage valve was closed to begin shearing. It is thought that the pore pressure build up was due to the phenomenon referred to as “undrained creep” by Head (1986). After the valve was closed, the piston had to travel into a seating groove in the top cap before making contact with the sample. Due to the very slow strain rates that were used, the drainage valve was often closed for a significant

time (up to 4 hours) before the piston made contact with the sample. The maximum pore pressure that developed during this time period due to undrained creep was approximately 2.7 psi. On average, the pore pressure in the sample at contact was about 1 psi.

In subsequent figures, the triaxial compression results are plotted as stress paths using both the MIT convention and the critical state convention. The variables p' and q, according to these conventions, are defined below:

MIT stress path convention:

$$p' = (\sigma_1' + \sigma_3')/2 \quad (3.2)$$

$$q = (\sigma_1' - \sigma_3')/2 \quad (3.3)$$

Critical state stress path convention:

$$p' = (\sigma_1' + \sigma_2' + \sigma_3')/3 \quad (3.4)$$

$$q = (\sigma_1' - \sigma_3') \quad (3.5)$$

where: σ_1' = major principal effective stress

σ_2' = intermediate principal effective stress

σ_3' = minor principal effective stress

The MIT convention is commonly used in the United States and is easily related to ϕ' and c'. The critical state convention is commonly used in many constitutive models, such as the Cam Clay model. The critical state p' is equal to the mean effective stress. The critical state q is equal to the deviator stress. The failure line in MIT p-q space is called the K_f line. The failure line in critical state p-q space is called the M line. The M line is the projection of the critical state line in p-q space.

The MIT and critical state stress paths for tests CU_3 through CU_9 are shown in Figure 3.12 through Figure 3.18. The deviator stress, excess pore pressure, and principal stress ratio (σ_1'/σ_3') are also plotted versus axial strain. The excess pore pressure includes the

excess pore pressure in the sample present due to undrained creep. Undrained creep produces an excess pore pressure plotted at zero axial strain.

The maximum principal stress ratio was used as the failure criterion for all of the CU tests. For a normally consolidated material with a linear failure envelope, the maximum principal stress ratio develops when the stress path is on the K_f line. In general, the stress paths are initially steep, then curve to the left and become relatively horizontal. Large excess pore pressures develop and the stress path either stops at the K_f line or travels up the K_f line. Most of the shear stress is mobilized at small axial strains.

The results of the CU tests on SB1 are summarized in Table 3.3. For the CU tests, the overconsolidation ratio (OCR) is the major principal effective stress at the end of consolidation (σ'_{1con}) divided by the major principal effective stress at the start of shear (σ'_{1shear}). A-bar is defined as the increase in excess pore pressure over increase in deviator stress. The excess pore pressure that occurs due to undrained creep prior to applying the deviator stress is not included in the A-bar calculation since it is not associated with the increase in deviator stress. For the normally consolidated tests, the average axial strain at failure was 6.5%; the average A-bar at failure was 2.0; and the average s_u/σ'_{1con} was 0.19.

Three CU tests (CU_11, CU_13, CU_14) were run on SB3. All of the samples were isotropically consolidated and sheared normally consolidated. The tests results are shown in Figure 3.19 through Figure 3.21. In general, the stress strain curves are initially steep, slight strain softening occurs until the stress paths hit the K_f line, then the stress paths travel up the K_f line. Failure is defined at the point when the stress path reaches the K_f line. The results of CU tests on SB3 are summarized in Table 3.4. For the three tests, the average OCR is 1.01; the average axial strain to failure is 3.4%; the average A-bar at failure is 2.2; and the average s_u/σ'_{1con} is 0.16.

Table 3.3 Isotropically Consolidated Undrained Triaxial Test Results for SB1

Test	σ'_{1con} (psi)	OCR	Water Content (%)	Void Ratio	Axial Strain at Failure (%)	A-bar at Failure	s_u (psi)	s_u / σ'_{1con}
CU_3	18.43	1.09	18.2	0.49	7.2	2.0	3.78	0.21
CU_4	5.13	1.06	22.0	0.60	6.3	2.1	0.83	0.16
CU_5	8.57	1.03	20.2	0.55	5.2	2.0	1.59	0.19
CU_6	5.12	1.09	22.0	0.60	5.0	2.0	0.90	0.18
CU_7	12.42	1.08	19.4	0.53	6.0	1.7	2.75	0.22
CU_8	39.1	1.32	16.2	0.44	7.5	1.5	7.70	0.20
CU_9	48.18	1.06	16.1	0.44	9.1	2.0	9.21	0.19
avg. of 3-7,9	NA	1.07	NA	NA	6.5	2.0	NA	0.19

Notes: σ'_{1con} = major principal effective stress at the end of consolidation
σ'_{1shear} = major principal effective stress at the beginning of shear
OCR = $\sigma'_{1con}/\sigma'_{1shear}$
A-bar = change in excess pore pressure / change in deviator stress
s_u = undrained shear strength, defined at maximum principal stress ratio
Water content and void ratio given at the end of consolidation

Table 3.4 Isotropically Consolidated Undrained Triaxial Test Results for SB3

Test	σ'_{1con} (psi)	OCR	Water Content (%)	Void Ratio	Axial Strain at Failure (%)	A-bar at Failure	s_u (psi)	s_u / σ'_{1con}
CU_11	8.41	1.00	21.6	0.57	2.4	2.2	1.46	0.17
CU_13	12.48	1.04	20.7	0.55	2.9	2.6	1.76	0.14
CU_14	20.36	1.00	19.8	0.52	4.9	2.3	3.5	0.17
avg.	NA	1.01	NA	NA	3.4	2.4	NA	0.16

Notes: σ'_{1con} = major principal effective stress at the end of consolidation
σ'_{1shear} = major principal effective stress at the beginning of shear
OCR = $\sigma'_{1con}/\sigma'_{1shear}$
A-bar = change in excess pore pressure / change in deviator stress
s_u = undrained shear strength, defined at maximum principal stress ratio
Water content and void ratio are reported at the end of consolidation

K_o Consolidated Undrained Triaxial Test

One K_o consolidation test (Ko_2) was run on SB1. The burette method described by Al-Hussaini (1981) was used. Al-Hussaini (1981) presents the results of four different methods of measuring K_o for sands in triaxial cells. The methods are 1) LVDT clamp with lateral strain sensor 2) strain gauge K_o belt 3) swinging arms lateral strain sensor and 4) burette method. Since the author concludes that all the tests give similar results, the burette method was used for test Ko_2 since it is the simplest method. The method involves monitoring the axial and volumetric strain and adjusting the cell pressure to maintain a K_o condition.

A stress path for the K_o consolidation and subsequent undrained shearing is shown in Figure 3.22. This figure illustrates the various stages of the test. A 2.8 inch diameter sample was prepared in a triaxial cell with initial specimen height of approximately 5.6 inches. The soil-bentonite was spooned inside a forming mold in the triaxial cell and first isotropically consolidated to 4 psi to point A inside the mold. After the 4 psi consolidation, it was decided to consolidate to a higher isotropic consolidation pressure of 16 psi to point B in order to take advantage of the higher coefficient of consolidation values exhibited at higher pressures in the consolidation tests. After final isotropic consolidation, the mold was left on and a deviator stress was applied in drained loading to bring the sample to an estimated value of K_o=0.5 at point C. Back pressure was not used in these stages and the volume of water expelled was measured with a graduated cylinder. After the sample had reached the estimated K_o state at point C, the sample was unloaded fully to point O. Next the drainage was closed on the specimen, the cell was disassembled, the forming mold was removed, and the sample dimensions were measured. The sample was reconsolidated to 4 psi to point A and backpressure saturated. A B-value of 0.95 was reached. The sample was then reconsolidated to 16 psi. A deviator stress was then applied in drained loading to bring the sample back to point C on the estimated K_o line.

The K_o consolidation was started at point C by continuing to apply the deviator stress at a constant strain rate and periodically increasing the cell pressure in order to maintain the condition of zero lateral strain. The portion of the K_o test from C to D was discounted for the following reasons: 1) inaccuracies in measuring axial deformations, and 2) strain rates were thought to be too high, which could have induced excess pore pressures in the sample. The strain rates were reduced from $2.7x10^{-3}$ %/min to $2.3x10^{-4}$ %/min at point D and the K_o consolidation test continued until point E.

During K_o consolidation, the volumetric strain and axial strain were measured. It was assumed that the sample deforms as a right circular cylinder. For a condition of no lateral strain, the area of the specimen is constant and the axial strain is equal to the volumetric strain. If the volumetric strain measured was greater than the axial strain measured, the ratio σ_3'/σ_1' was decreased. This was achieved by increasing the cell pressure in smaller increments or less frequently under the constant axial strain rate. The results of the K_o consolidation are shown in Figure 3.23 for the stress path from point D to point E. The strains were measured starting from point D. At points where the ratio of the volumetric strain to the axial strain was equal to one, the values of σ_3'/σ_1' were noted. These values gave an average value of K_o equal to 0.57. The K_o condition is shown in the figure with the dotted line. The dotted line shows that the test from point D to point E roughly followed the K_o line in a step-wise fashion.

After K_o consolidation, the sample was sheared undrained as test CU_15, which is shown in Figure 3.24. The stress path for CU_15 is the portion of the path from point E (after K_o consolidation) to point F (at the K_f line) in Figure 3.22. The stress path in Figure 3.24 shows that the deviator stress peaks after a small axial strain and then strain softening occurs until the stress path reaches the K_f line. The peak occurs after the addition of 4.1 psi of deviator stress at an axial strain of 0.07%. When the stress path reaches the K_f line, the deviator stress has dropped 2.8 psi below the deviator stress at the end of the K_o

consolidation. Similar strain softening behavior is reported by Ladd et al. (1977) for K_o consolidated plane strain compression tests. Small strains to failure (0.4% for lean clays) were also observed by the authors. The results of Ko_2 and CU_15 are shown in Table 3.5. Failure was evaluated at both peak deviator stress and maximum principal stress ratio. The s_u/σ'_{1con} ratio for the respective failure criteria are 0.21 and 0.25.

Table 3.5. K_o Consolidated Undrained Triaxial Test on SB1

Test	K_o	σ'_{1con} (psi)	σ'_{3con} (psi)	OCR	Water Content (%)	Void Ratio
Ko_2, CU_15	0.57	73.50	40.20	1.00	15.3	0.41

Test	Failure Criterion	Axial Strain at Failure (%)	A-bar at Failure	s_u (psi)	s_u / σ'_{1con}
CU_15	Peak Deviator Stress	6.4	-10.0	15.1	0.21
	Max. psr	0.07	0.95	18.7	0.25

Notes: σ'_{1con} = major principal effective stress at the end of consolidation
σ'_{3con} = minor principal effective stress at the beginning of shear
OCR = $\sigma'_{1con}/\sigma'_{1shear}$
σ'_{1shear} = major principal effective stress at the beginning of shear
A-bar = change in excess pore pressure / change in deviator stress
s_u = undrained shear strength, defined at maximum principal stress ratio
psr = principal stress ratio = σ'_1/σ'_3
Water content and void ratio reported at the end of consolidation

Summary of Undrained Triaxial Tests

All of the stress paths for the CU tests on SB1 are shown in Figure 3.25. Both the MIT stress paths and the critical state stress paths are shown. All of the tests create a single linear strength envelope. Dotted lines are used to show the K_f line with the MIT stress paths and the M line with the critical state stress paths. The angle that the K_f line makes

with the horizontal is called alpha, α', and the intercept is called d'. These variables can be related to ϕ' and c' by the following equations:

$$\tan\alpha' = \sin\phi' \tag{3.6}$$

$$c' = \frac{d'}{\cos\phi'} \tag{3.7}$$

The slope of the M line is the critical state parameter M. For the case of triaxial compression, M is related to ϕ' by the following equation (Wood 1990):

$$M = \frac{6\sin\phi'}{3-\sin\phi'} \tag{3.8}$$

All of the stress paths for the CU tests on SB3 are shown in Figure 3.26. Again, the tests create a single linear strength envelope. The strength envelope for SB3 is the same as for SB1. The resulting undrained strength parameter values for SB1 and SB3 are listed in Table 3.6.

Table 3.6 Undrained Strength Parameter Values for SB1 and SB3

Soil-Bentonite Mixture	ϕ' (degrees)	c' (psi)	α' (degrees)	d' (psi)	M
SB1	32	0	28	0	1.3
SB3	32	0	28	0	1.3

Isotropically Consolidated Drained Triaxial Tests

Nine isotropically consolidated drained triaxial tests (CD_1 through CD_8 and CD_10) were performed on SB1. Two CD tests (CD_11 and CD_12) were run on SB3. The tests on SB1 were designed to determine constitutive model parameters. Tests CD_1, CD_8, and CD_10 were run on isotropically consolidated samples which were sheared normally consolidated to failure to find the strength envelope and the parameter values for the hyperbolic model described by Duncan and Chang (1970). Tests CD_2 through CD_7 were sheared overconsolidated in order to gain information on the yield surface and plastic

potential surface. All of these tests were isotropically consolidated to 20 psi, then re-bounded isotropically to various overconsolidation ratios. A few of these tests were not run to failure (CD_3 and CD_4). The tests on SB3 were run on isotropically consolidated samples that were sheared to failure. Except for tests CD_3 and CD_4, the test results are presented in this chapter. Interpretation of the tests to determine constitutive model parameters is discussed in Chapter 4.

The test results for SB1 are shown in Figure 3.27 through Figure 3.33. Tests CD_3 and CD_4 are not shown since they were not run to failure. The MIT and critical state stress paths are shown in the figures. The deviator stress and volumetric strain are plotted versus axial strain. The specific volume is plotted versus mean effective stress. The specific volume is defined as 1 plus the void ratio. It is a convenient parameter that is commonly used in critical state models (Wood 1990).

For a CD test, since σ'_3 is constant, the MIT stress path rises at a 1 on 1 slope and the critical state stress path rises at a 3 on 1 slope (Wood 1990). From Figure 3.27, it can be seen that the stress path for test CD_1 rises in a slightly crooked fashion. This is due to varying levels of pore water in the outflow burette. In subsequent tests, the burette was emptied frequently to keep the water in the outflow burette fairly constant.

The normally consolidated tests (CD_1, CD_8, CD_10) have gradually sloping stress strain curves. The overconsolidated tests have initially steep stress strain curves. A change in compressibility after yield in the overconsolidated samples can be seen from the specific volume plots. A negative volumetric strain value signifies volumetric expansion or dilation. All samples are contractive except for the most overconsolidated samples CD_6 and CD_7. Both CD_6 and CD_7 initially contract and then dilate. A summary of the CD tests performed on SB1 is given in Table 3.7.

Table 3.7 Isotropically Consolidated Drained Triaxial Test Results for SB1

Test	σ'_{1con} (psi)	OCR at Start of Shear	σ'_3 at Failure (psi)	σ'_1 at Failure (psi)	Axial Strain at Failure (%)	Water Content at Failure (%)	Void Ratio at Failure
CD_1	14.33	1.0	14.28	46.49	19.8	15.16	0.411
CD_2	20.47	3.1	6.71	21.29	16.7	16.43	0.445
CD_3	20.48	1.4	14.56	NA	NA	NA	NA
CD_4	20.46	1.1	18.56	NA	NA	NA	NA
CD_5	20.36	1.9	10.54	35.12	21.7	15.93	0.432
CD_6	20.52	7.8	2.63	8.88	6.75	18.80	0.510
CD_7	20.48	8.0	2.56	9.43	11.4	18.46	0.500
CD_8	6.34	1.0	6.34	19.19	21.1	17.32	0.469
CD_10	25.38	1.0	25.38	86.06	19.7	13.94	0.378

Notes: σ'_{1con} = major principal effective stress at the end of consolidation
OCR = $\sigma'_{1con}/\sigma'_{1shear}$
σ'_{1shear} = major principal effective stress at the beginning of shear

Two CD tests (CD_11 and CD_12) were run on SB3. The samples were isotropically consolidated and sheared normally consolidated. The test results are shown in Figure 3.34 and Figure 3.35. The deviator stress versus axial strain plots look similar to CD tests on normally consolidated samples of SB1. Both SB3 samples reach a maximum deviator stress at approximately 17% axial strain. Both samples are initially contractive, and then exhibit dilation at approximately 11%. Dilation was not measured in normally consolidated CD tests on SB1. Under similar confining pressures, SB3 exhibits less volumetric strain than SB1. SB3 was also shown to be less compressible than SB1 in 1-D consolidation tests. A summary of the CD tests performed on SB3 is shown in Table 3.8.

The CD strength envelopes for SB1 and SB3 are shown in Figure 3.36 and Figure 3.37. Only the tests that were normally consolidated or normally consolidated at failure are shown. For SB1, the effective friction angle, ϕ', is 32 degrees and the cohesion is zero. For SB3, the effective friction angle, ϕ', is 33 degrees, and the cohesion is zero. The drained strength parameter values are listed in Table 3.9. These friction angles found from

the CD tests are within one degree of those found from the CU tests and are consistent with the range of values found for soil-bentonite in the literature (ϕ'=31 to 33 degrees).

Table 3.8 Isotropically Consolidated Drained Triaxial Test Results for SB3

Test	σ'_{1con} (psi)	OCR at Start of Shear	σ'_3 at Failure (psi)	σ'_1 at Failure (psi)	Axial Strain at Failure (%)	Water Content at Failure (%)	Void Ratio at Failure
CD_11	10.00	1.0	10.28	35.78	16.4	18.79	0.498
CD_12	13.31	1.0	13.59	48.50	18.2	18.47	0.489

Notes: σ'_{1con} = major principal effective stress at the end of consolidation
OCR = $\sigma'_{1con}/\sigma'_{1shear}$
σ'_{1shear} = major principal effective stress at the beginning of shear

Table 3.9 Drained Strength Parameter Values for SB1 and SB3

Soil-Bentonite Mixture	ϕ' (degrees)	c' (psi)	α' (degrees)	d' (psi)	M
SB1	32	0	28	0	1.3
SB3	33	0	29	0	1.3

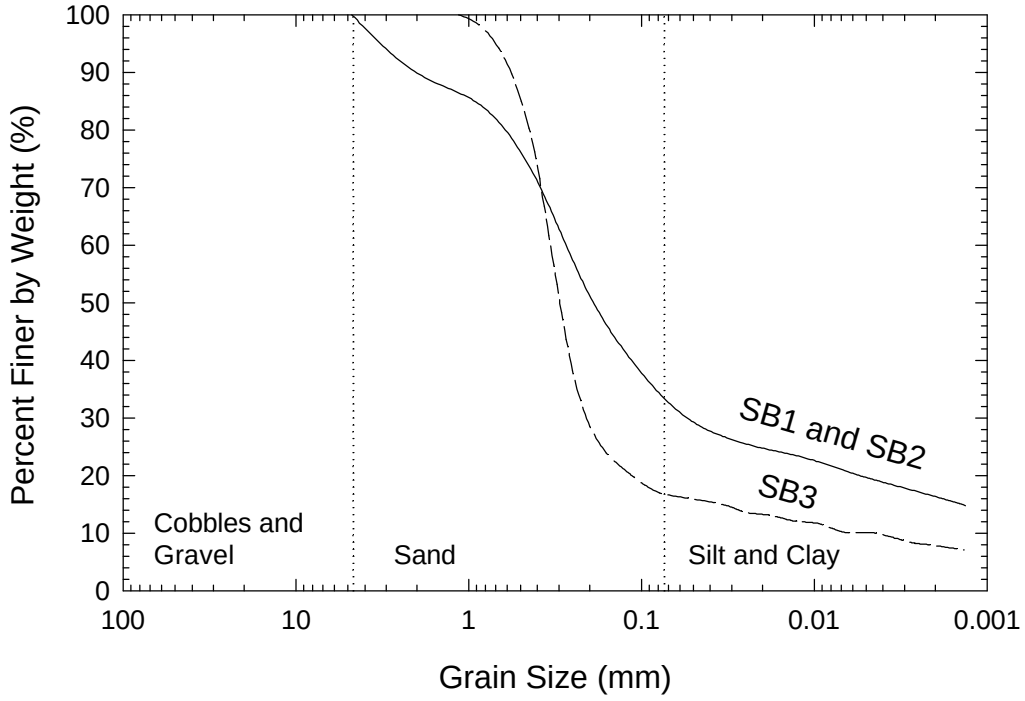

Figure 3.1 Grain Size Distributions of SB1, SB2, and SB3

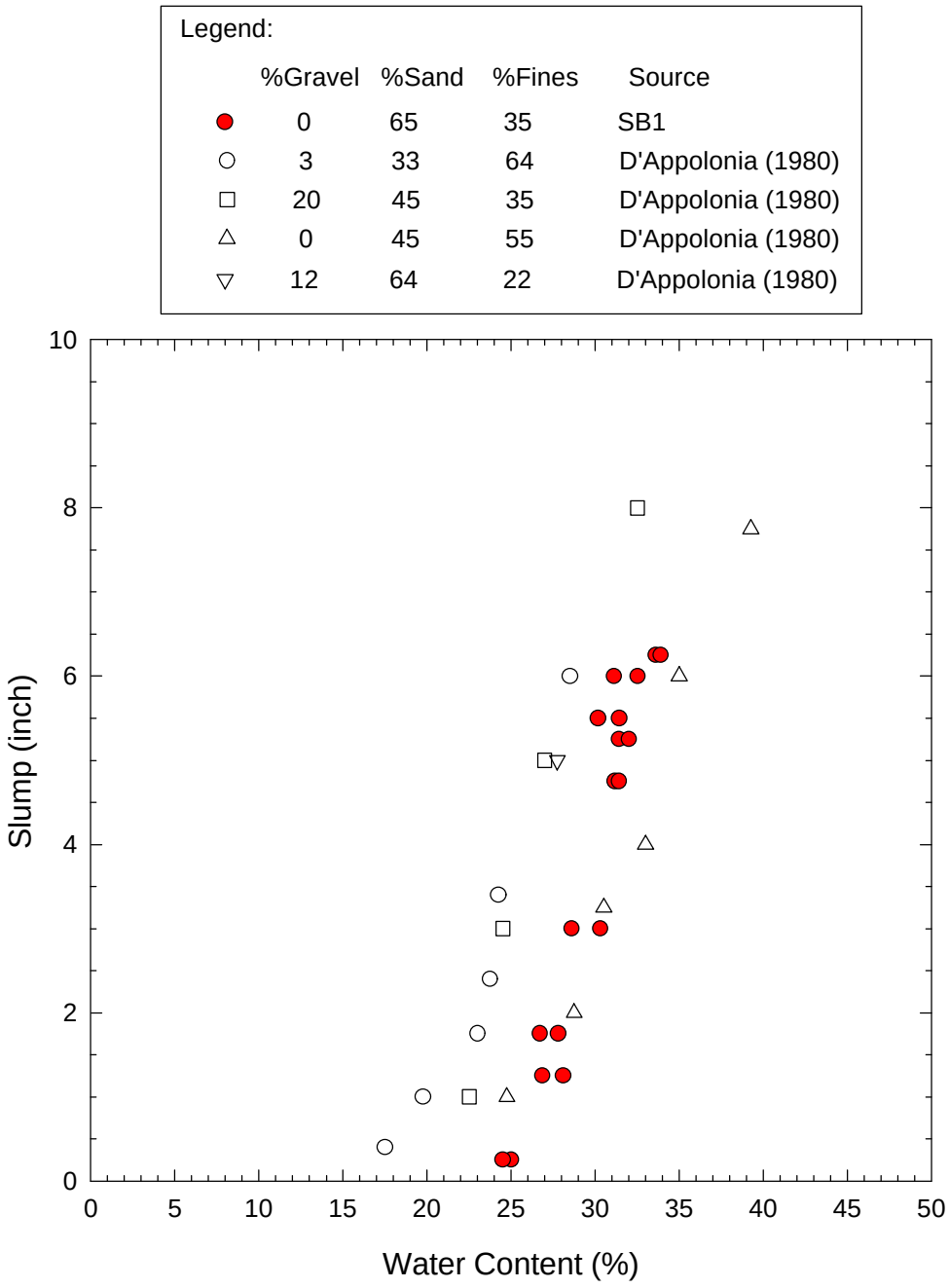

Figure 3.2 Slump Versus Water Content for Various Soil-Bentonite Mixtures

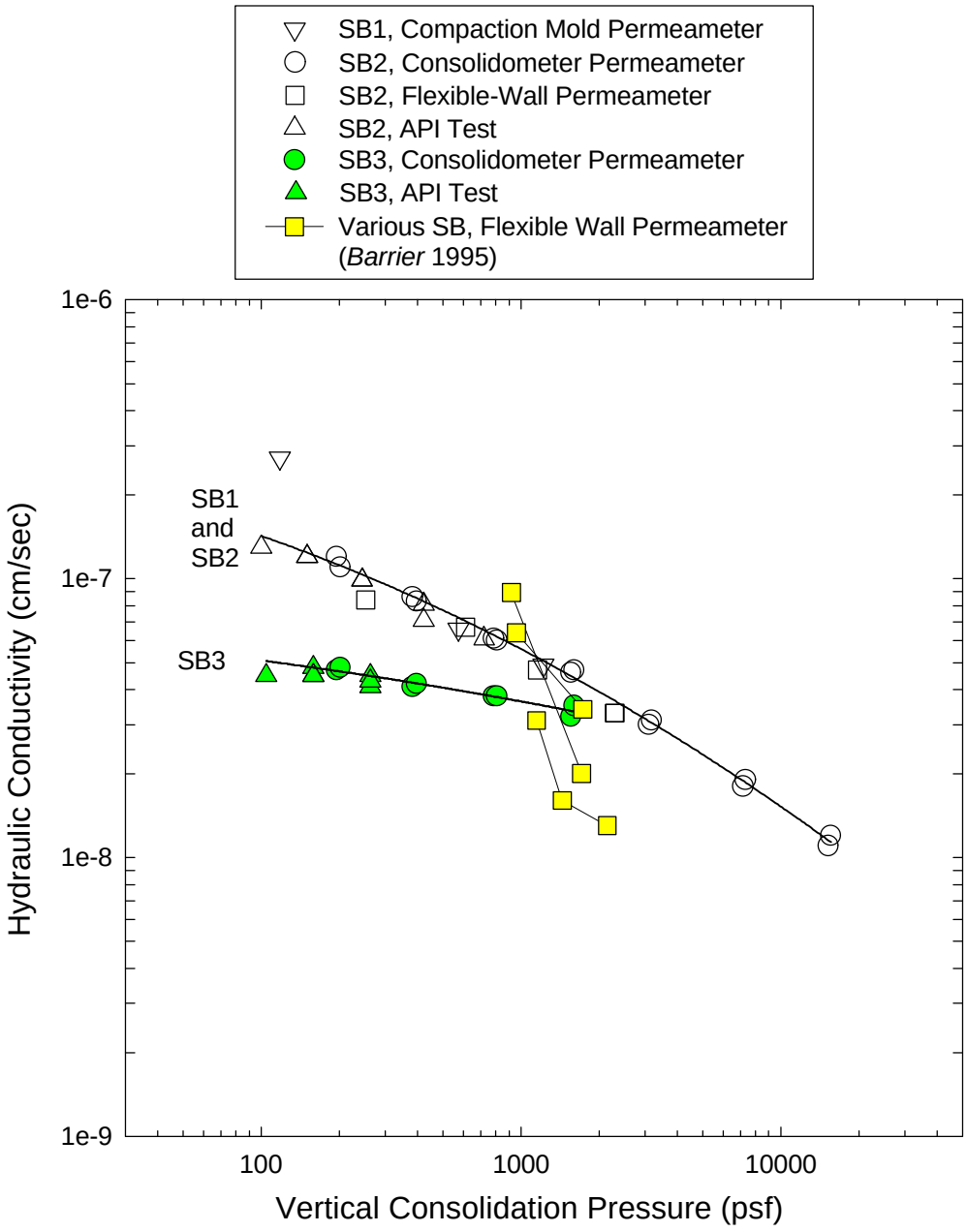

Figure 3.3 Hydraulic Conductivity Results for Various Soil-Bentonite Mixtures

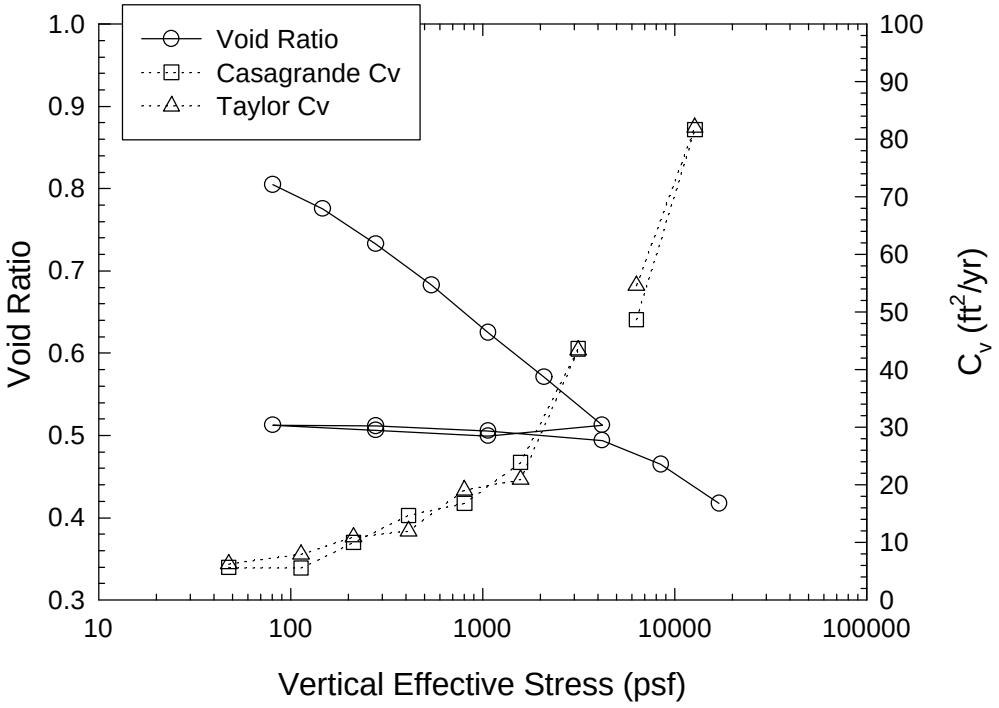

Figure 3.4 One-Dimensional Consolidation Test C5 on SB1

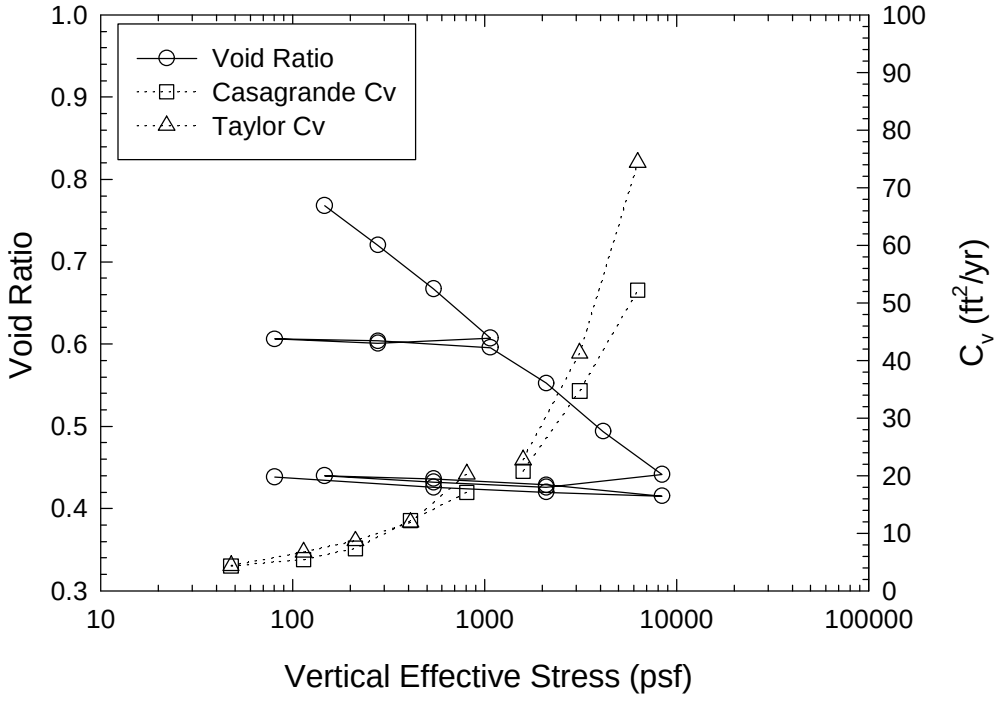

Figure 3.5 One-Dimensional Consolidation Test C6 on SB1

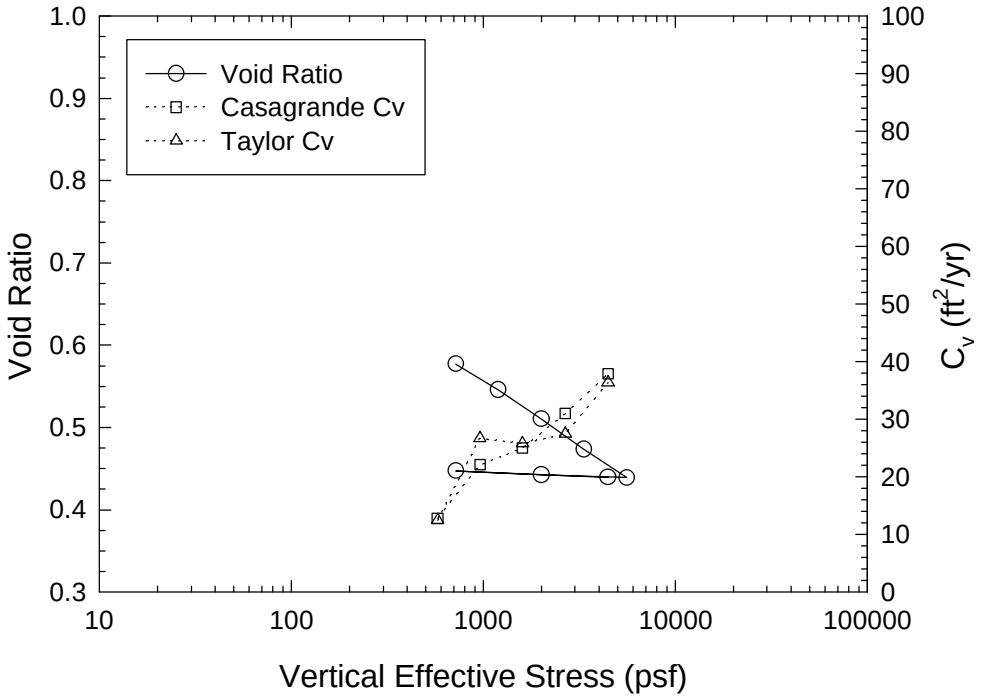

Figure 3.6 Isotropic Consolidation Test IC_1 on SB1

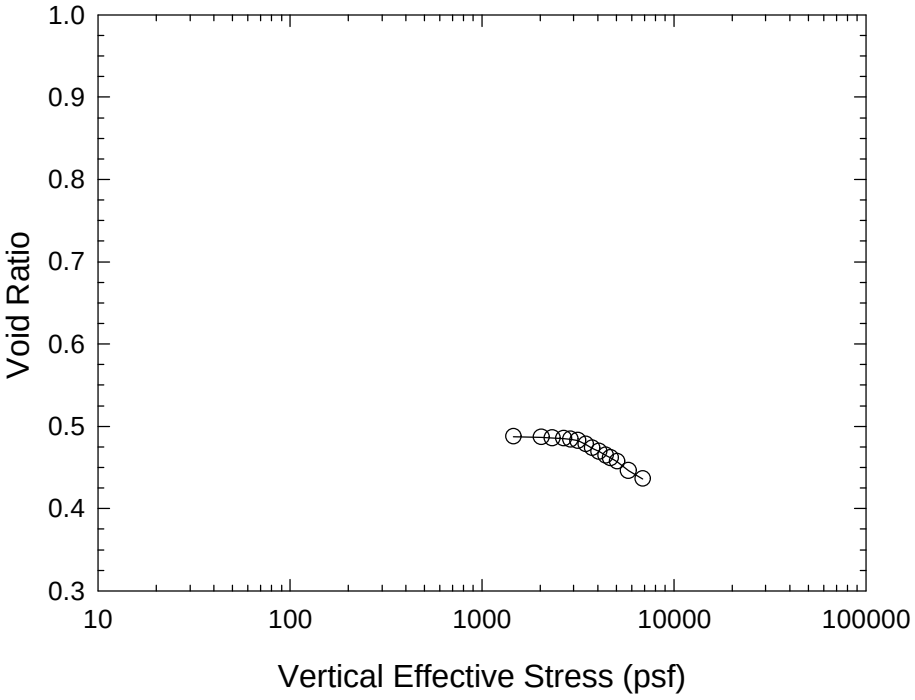

Figure 3.7 Isotropic Consolidation Test IC_2 on SB1

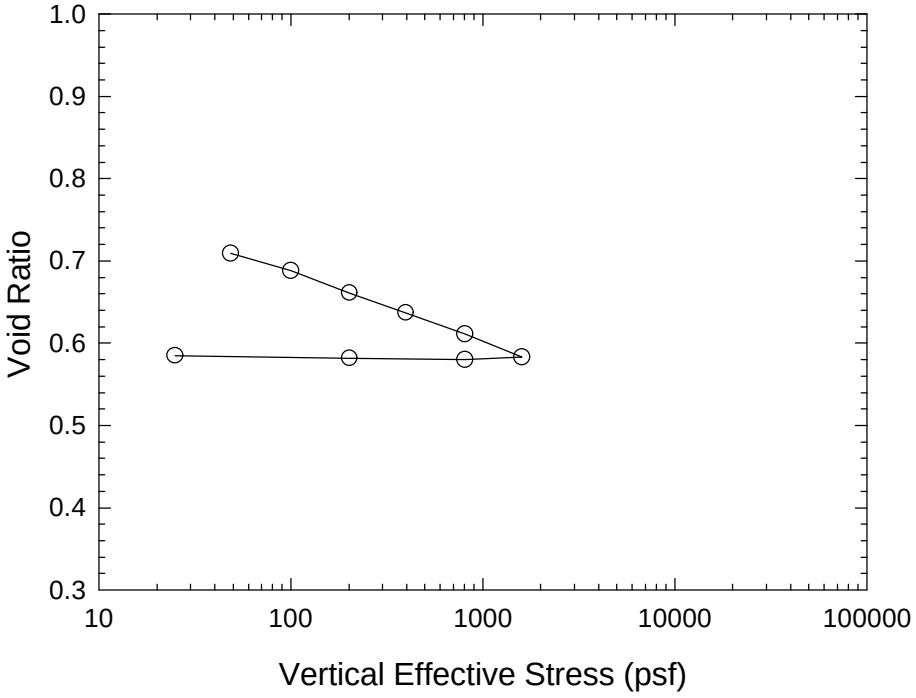

Figure 3.8 One-Dimensional Consolidation Test CP5 on SB3

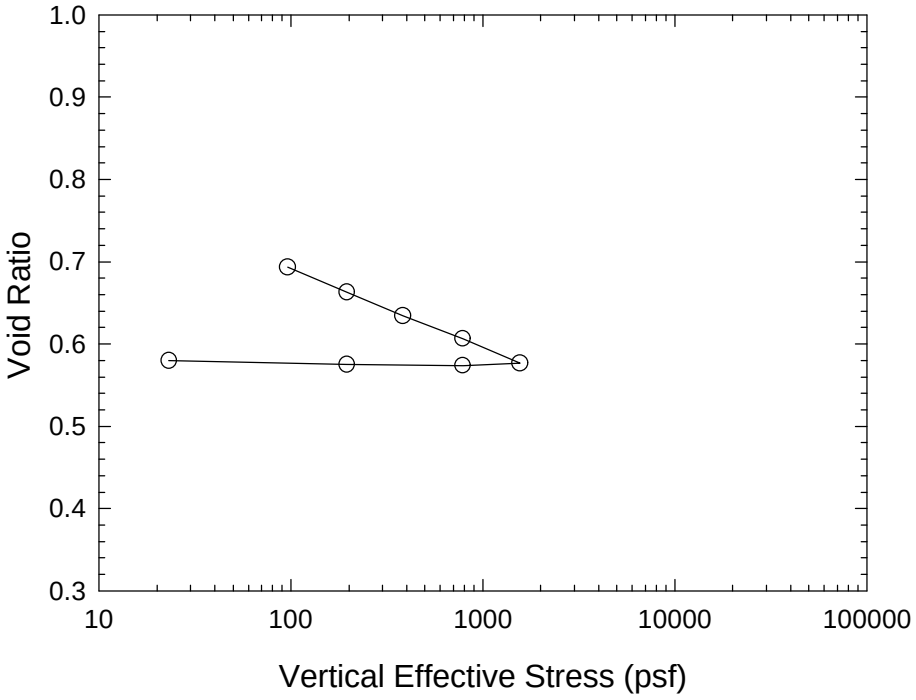

Figure 3.9 One-Dimensional Consolidation Test CP6 on SB3

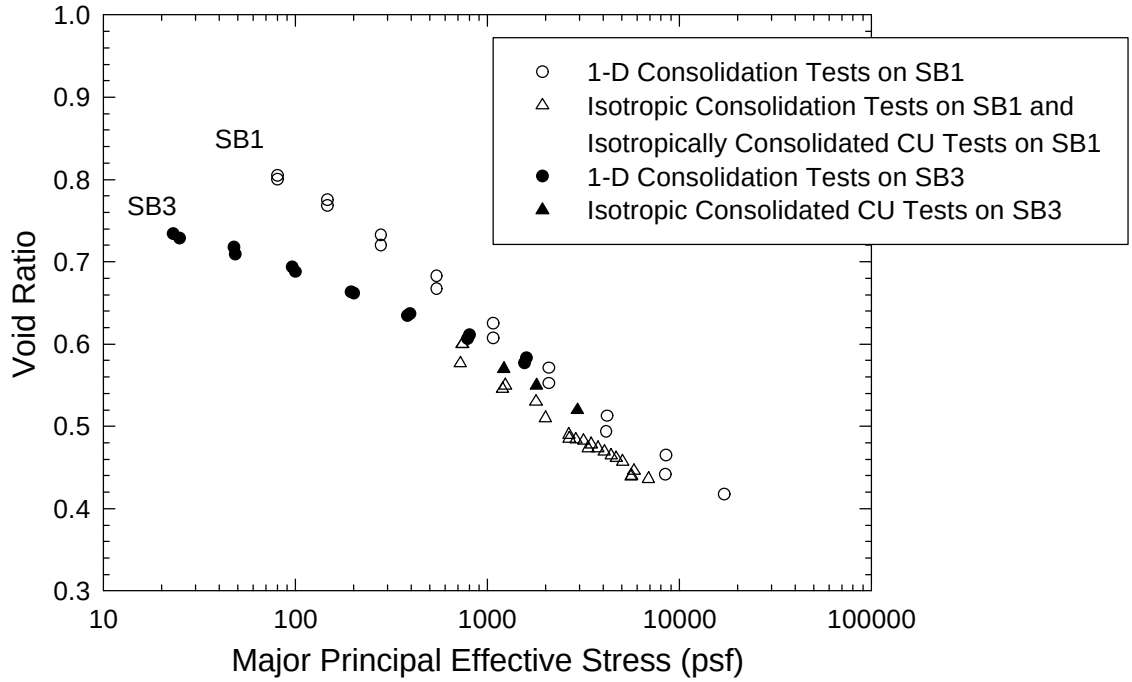

Figure 3.10 Major Principal Effective Stress Versus Void Ratio for Consolidation Tests on SB1 and SB3

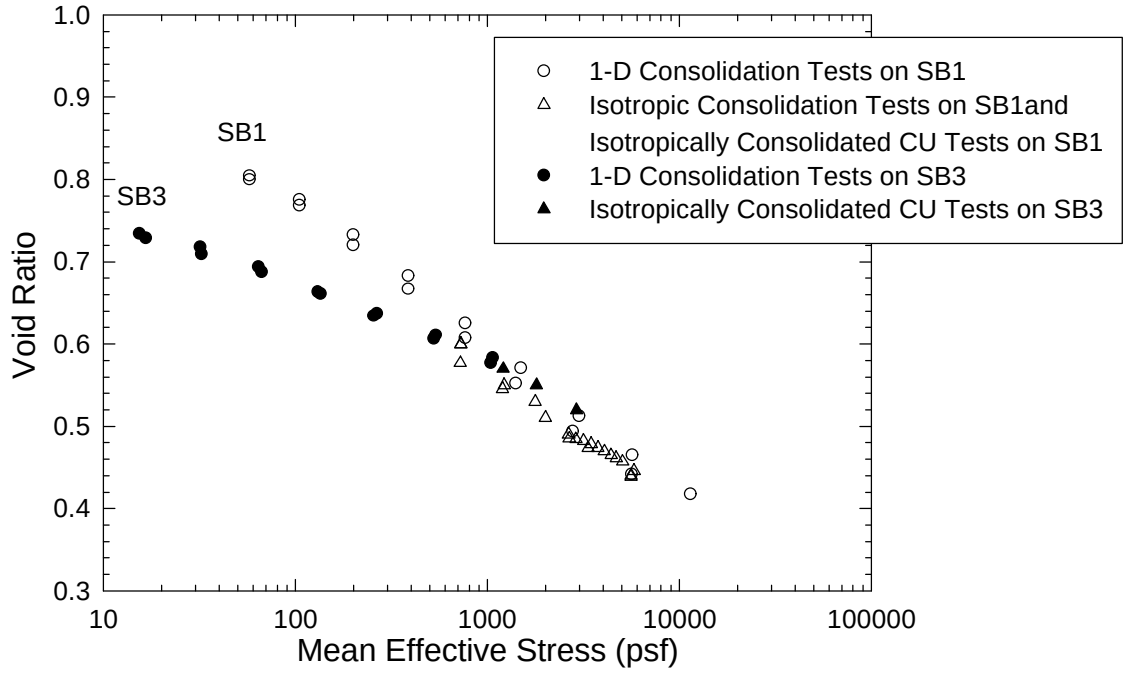

Figure 3.11 Mean Effective Stress Versus Void Ratio for Consolidation Tests on SB1 and SB3

Test CU_3 on SB1
σ'_{1con} = 18.43 psi
Sheared at OCR=1.09

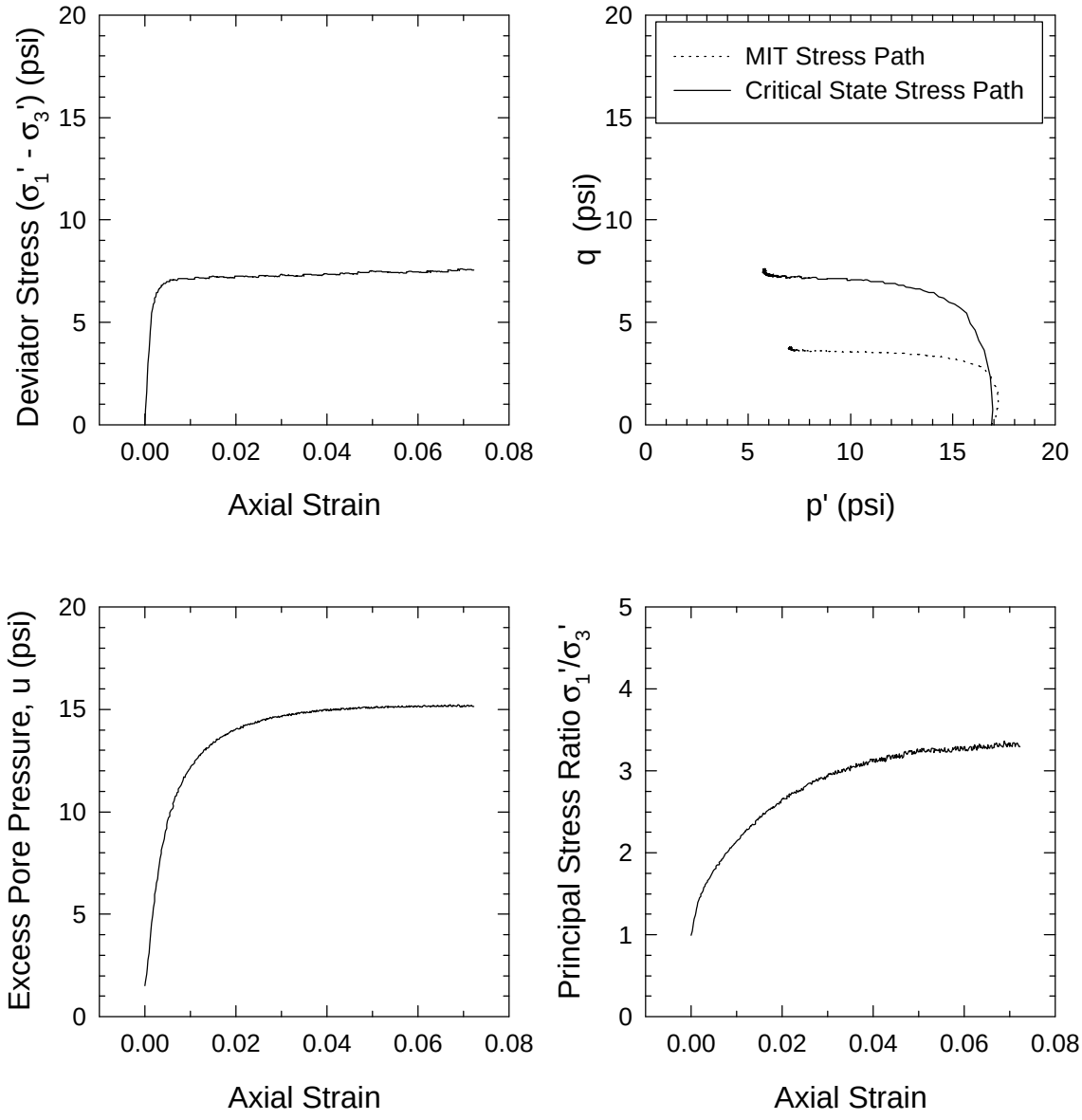

Figure 3.12 Consolidated Undrained Triaxial Test CU_3 on SB1

Test CU_4 on SB1
σ'_{1con}= 5.13 psi
Sheared at OCR=1.06

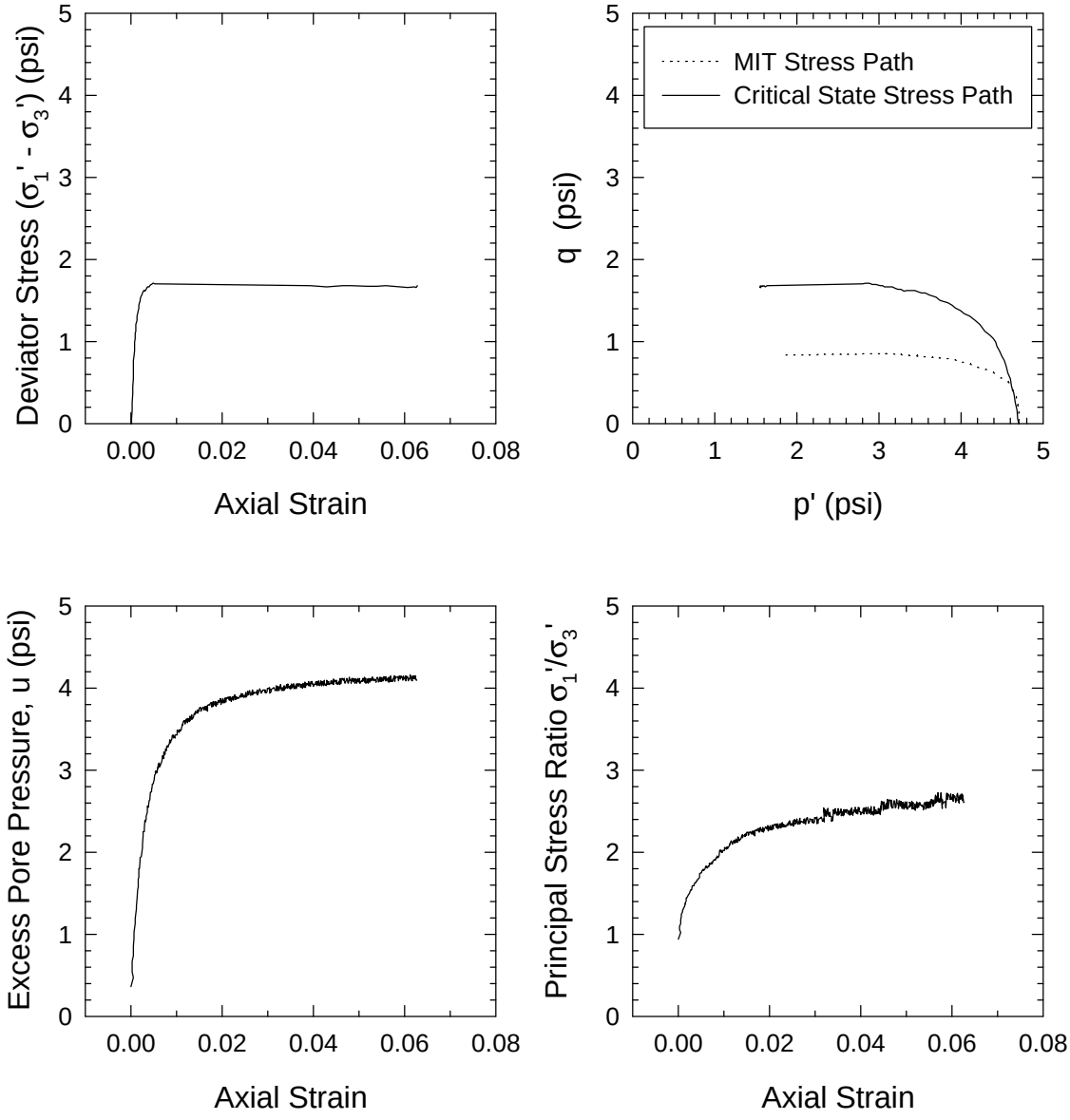

Figure 3.13 Consolidated Undrained Triaxial Test CU_4 on SB1

Test CU_5 on SB1
σ'_{1con}=8.57 psi
Sheared at OCR=1.03

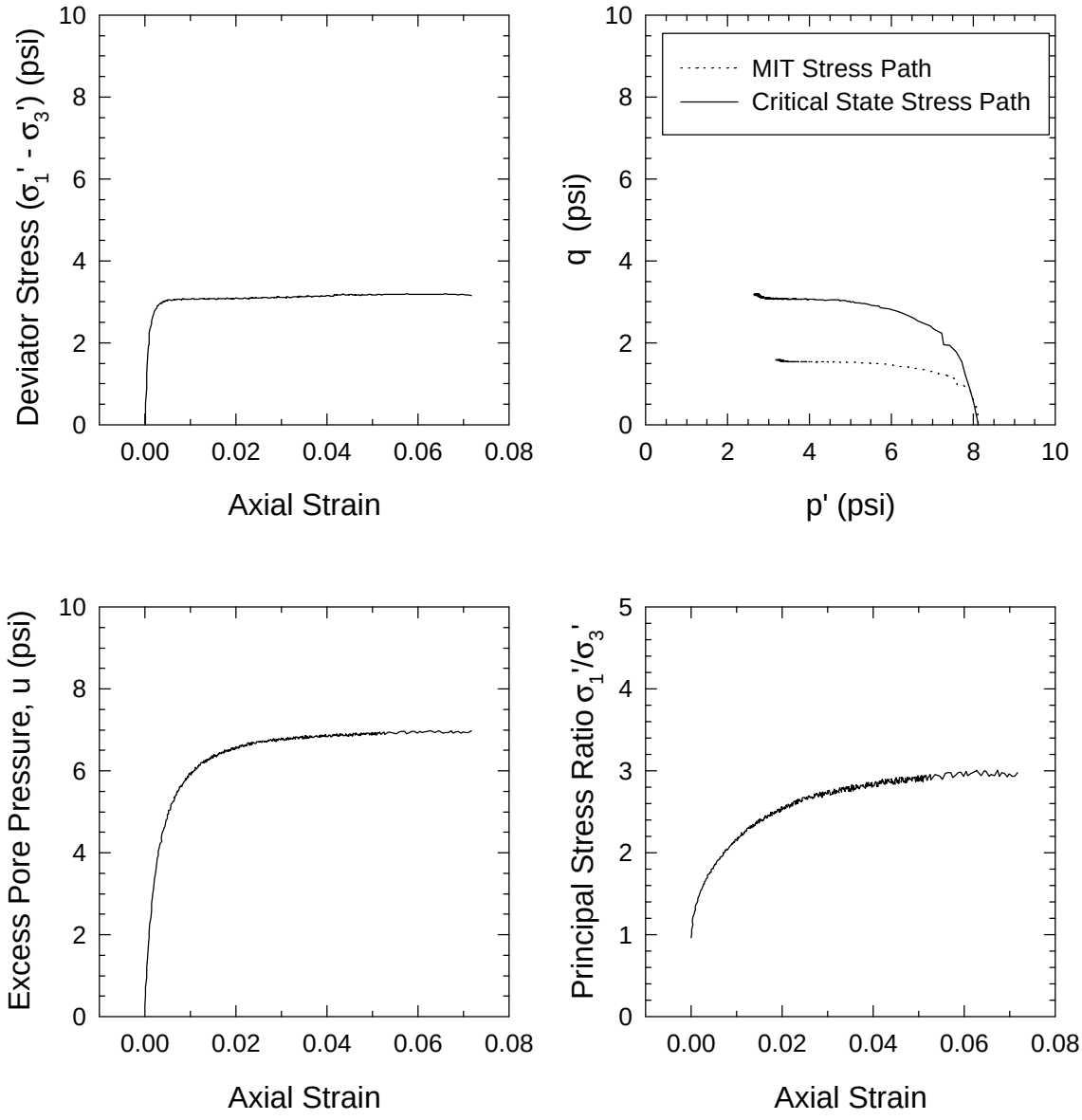

Figure 3.14 Consolidated Undrained Triaxial Test CU_5 on SB1

Test CU_6 on SB1
σ'_{1con}= 5.12 psi
Sheared at OCR=1.09

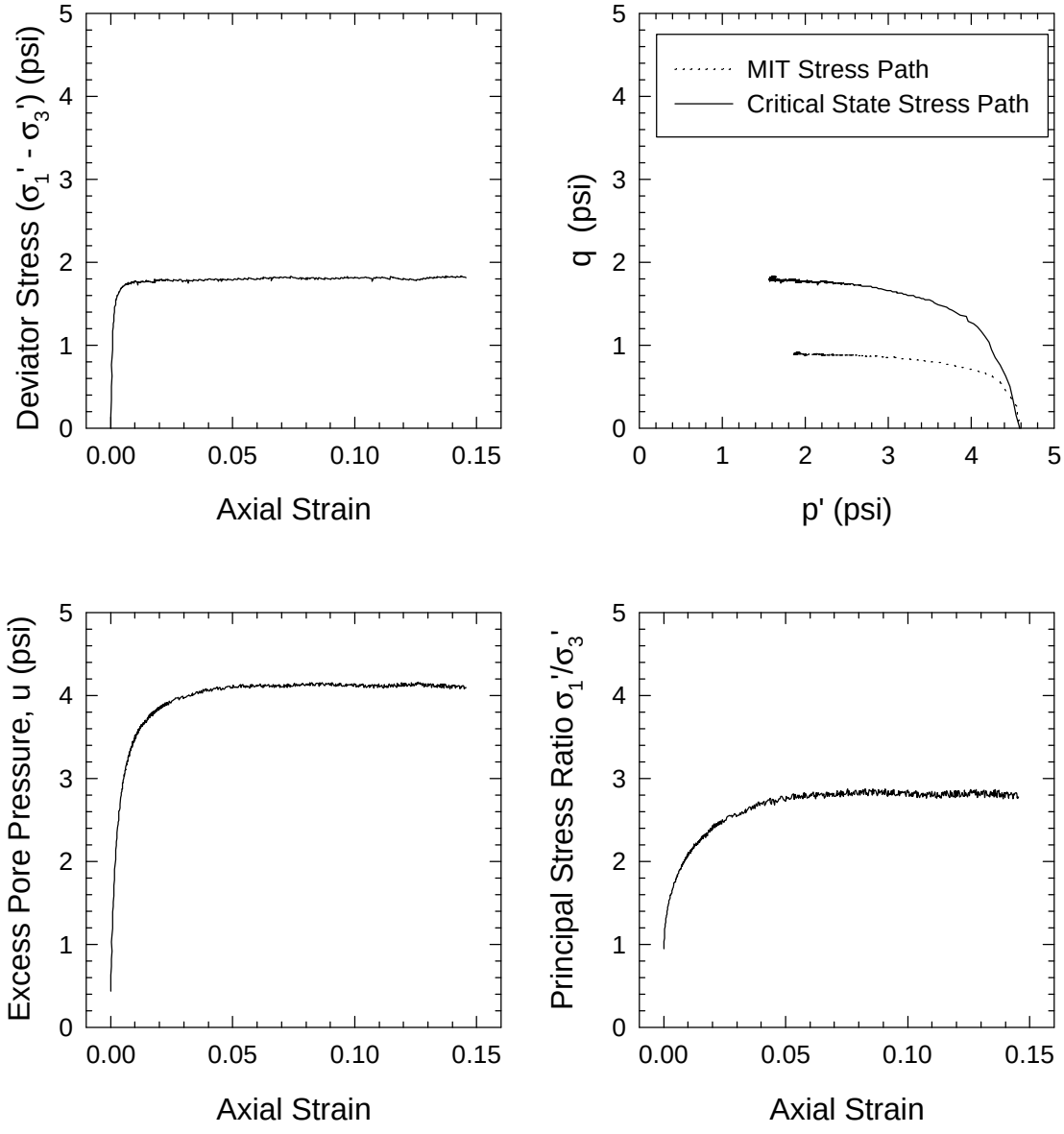

Figure 3.15 Consolidated Undrained Triaxial Test CU_6 on SB1

Test CU_7 on SB1
σ'_{1con}=12.42 psi
Sheared at OCR=1.08

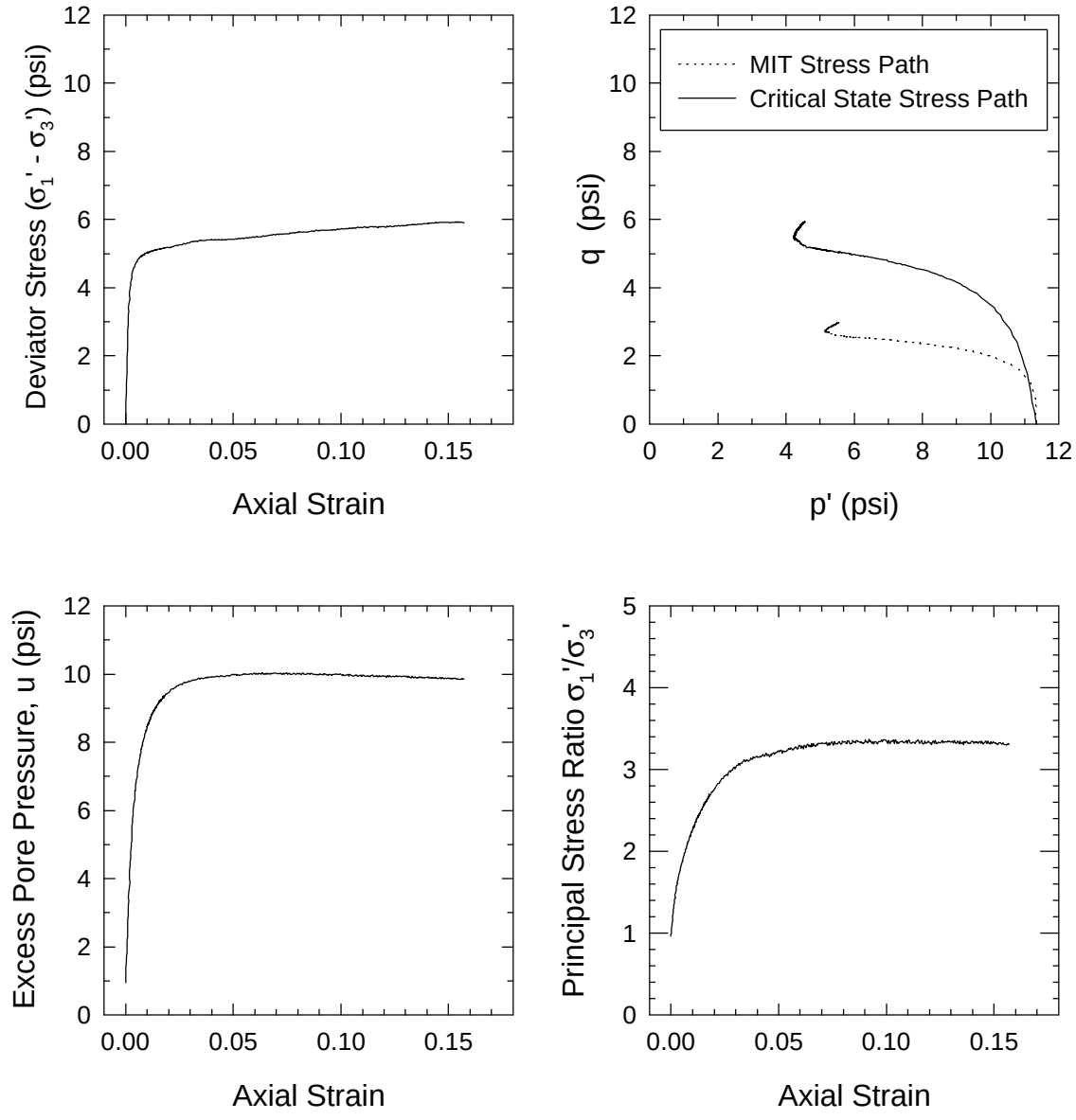

Figure 3.16 Consolidated Undrained Triaxial Test CU_7 on SB1

Test CU_8 on SB1
σ'_{1con}= 39.1 psi
Sheared at OCR=1.32

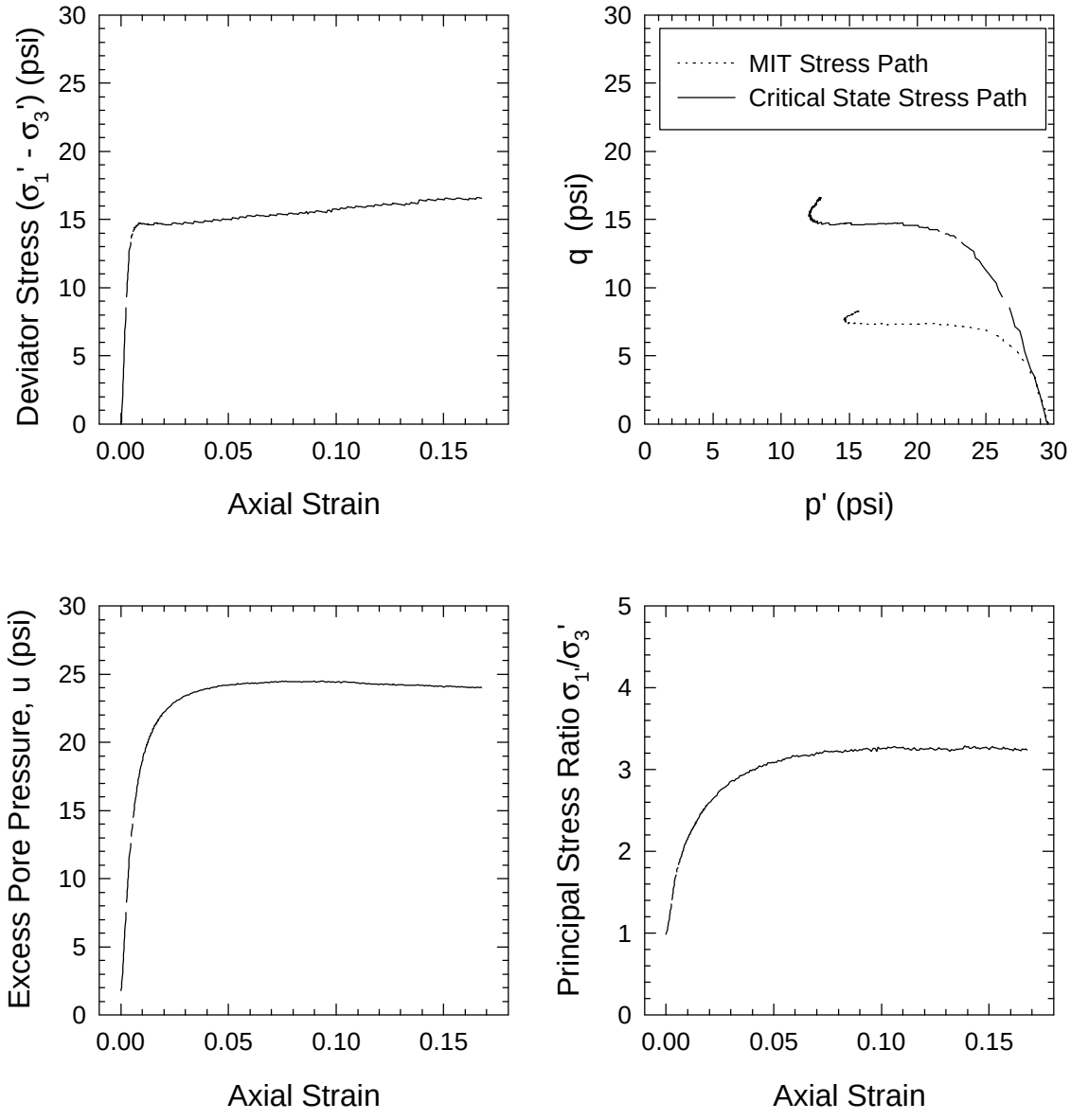

Figure 3.17 Consolidated Undrained Triaxial Test CU_8 on SB1

Test CU_9 on SB1
σ'_{1con}= 47.78 psi
Isotropically Consolidated as IC_2 and Sheared at OCR=1.06 as CU_9

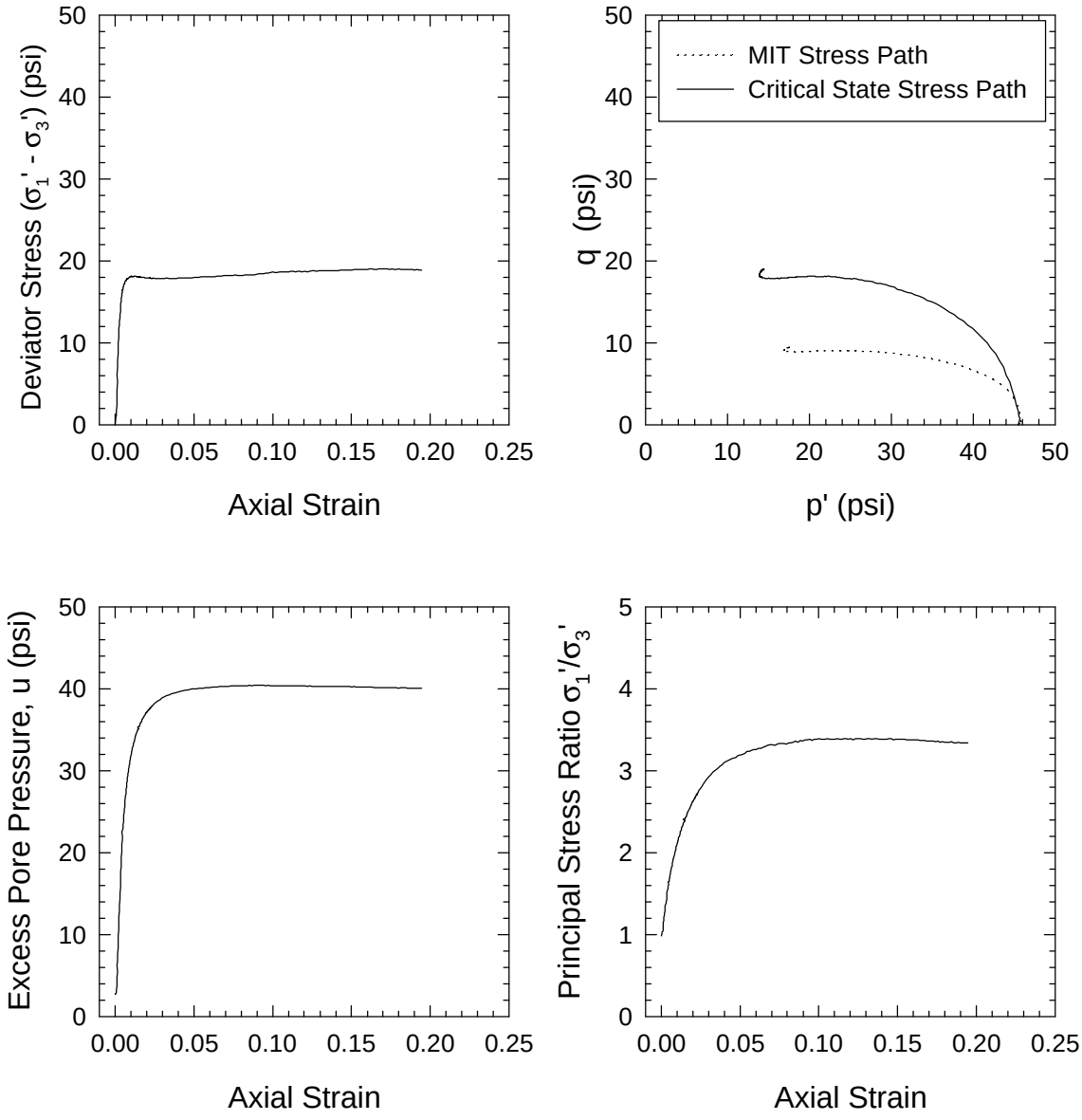

Figure 3.18 Consolidated Undrained Triaxial Test CU_9 on SB1

Test CU_11 on SB3
σ'_{1con}=8.41 psi
Sheared at OCR=1.06

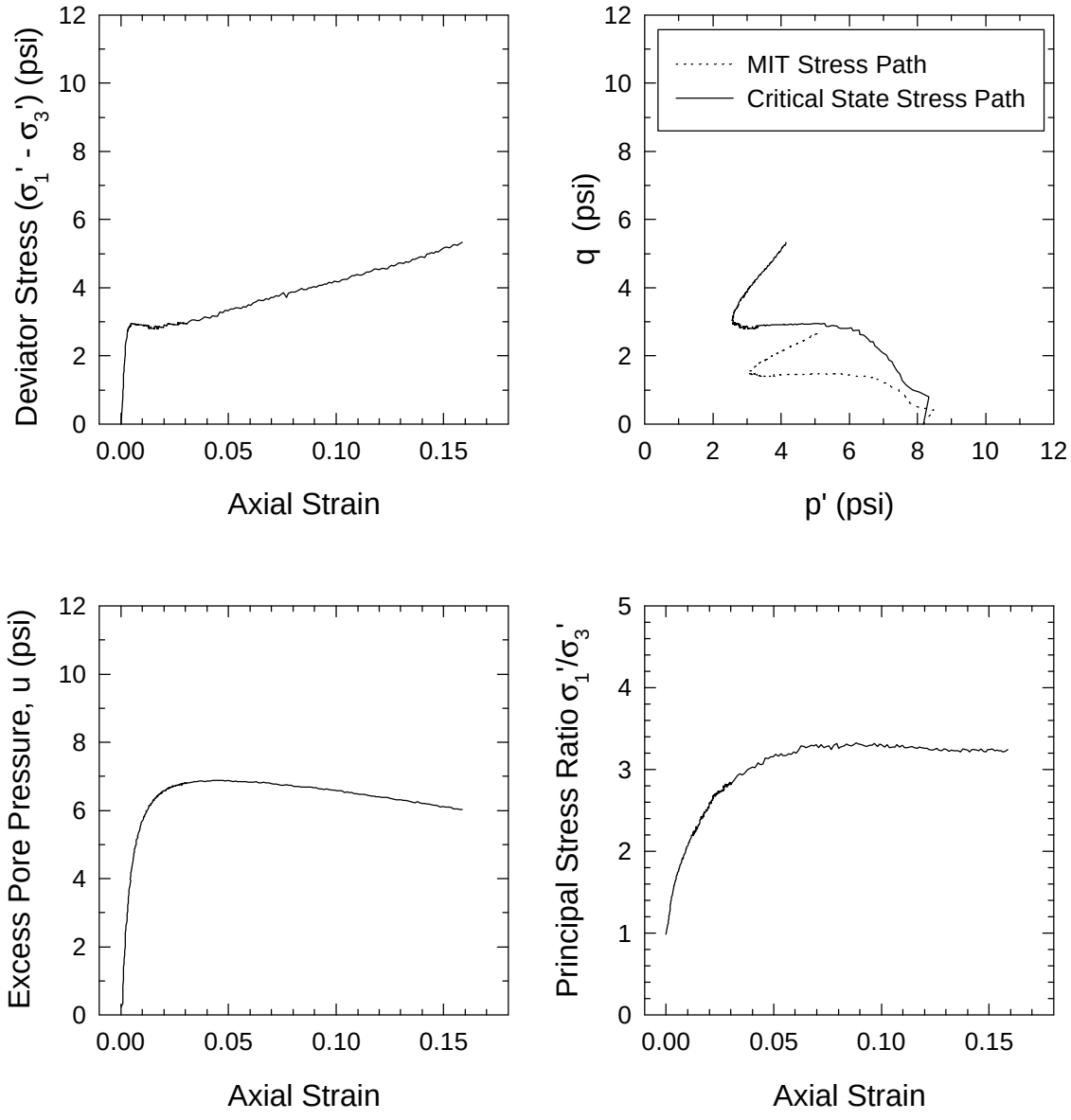

Figure 3.19 Consolidated Undrained Triaxial Test CU_11 on SB3

Test CU_13 on SB3
σ'_{1con}= 12.48 psi
Sheared at OCR=1.04

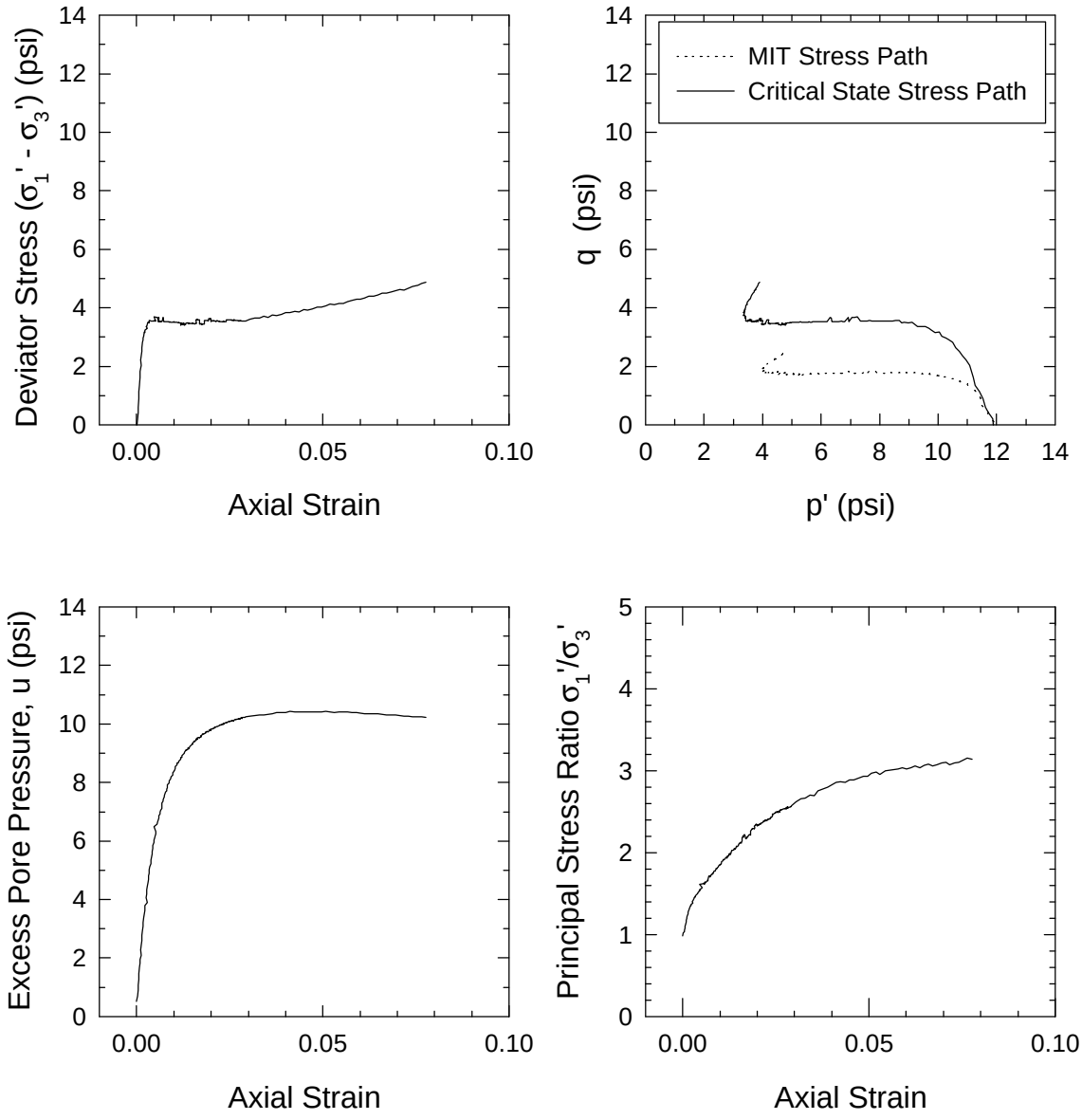

Figure 3.20 Consolidated Undrained Triaxial Test CU_13 on SB3

Test CU_14 on SB3
σ'_{1con}=20.36 psi
Sheared at OCR = 1.00

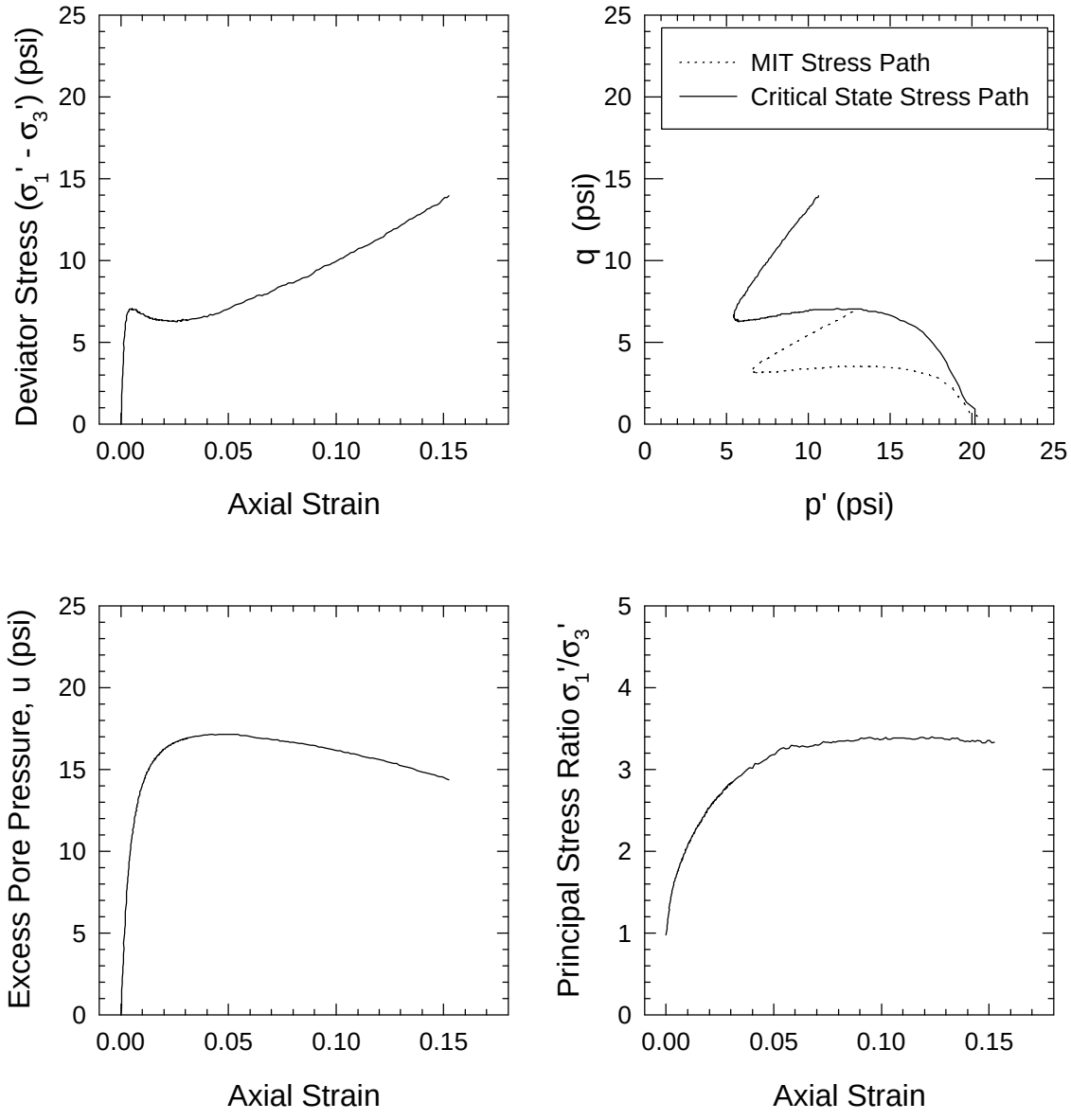

Figure 3.21 Consolidated Undrained Triaxial Test CU_14 on SB3

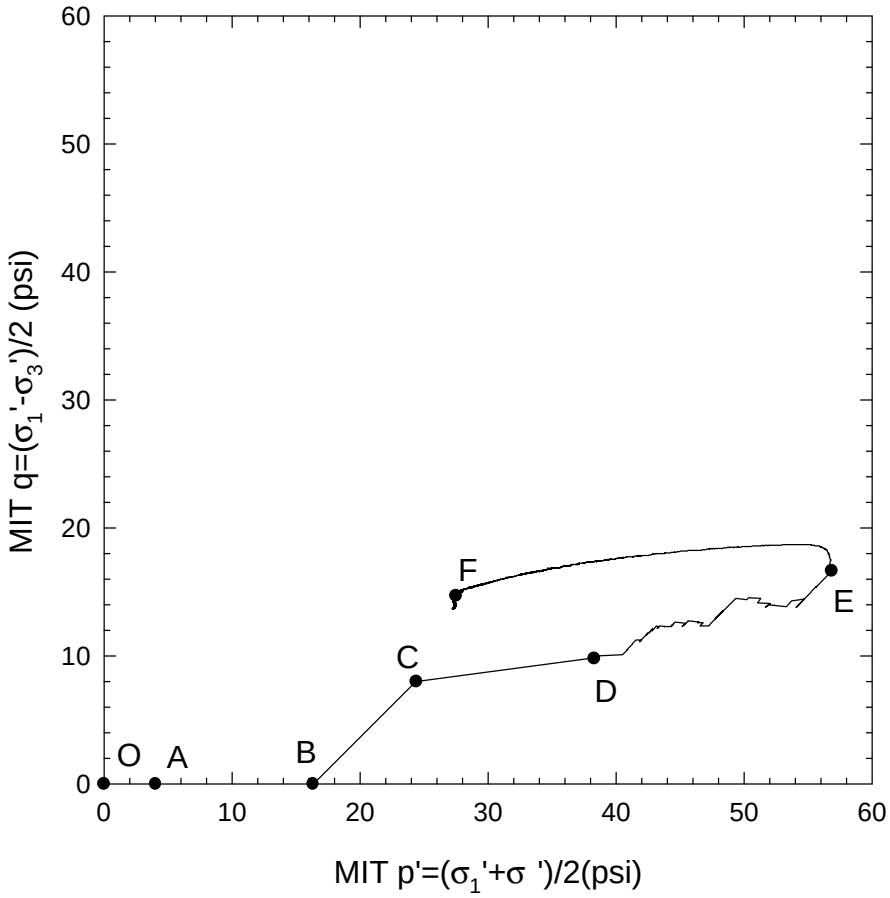

Figure 3.22 Combined Stress Path for K_o Consolidation Test Ko_2 on SB1 Subsequently Sheared Undrained as Test CU_15

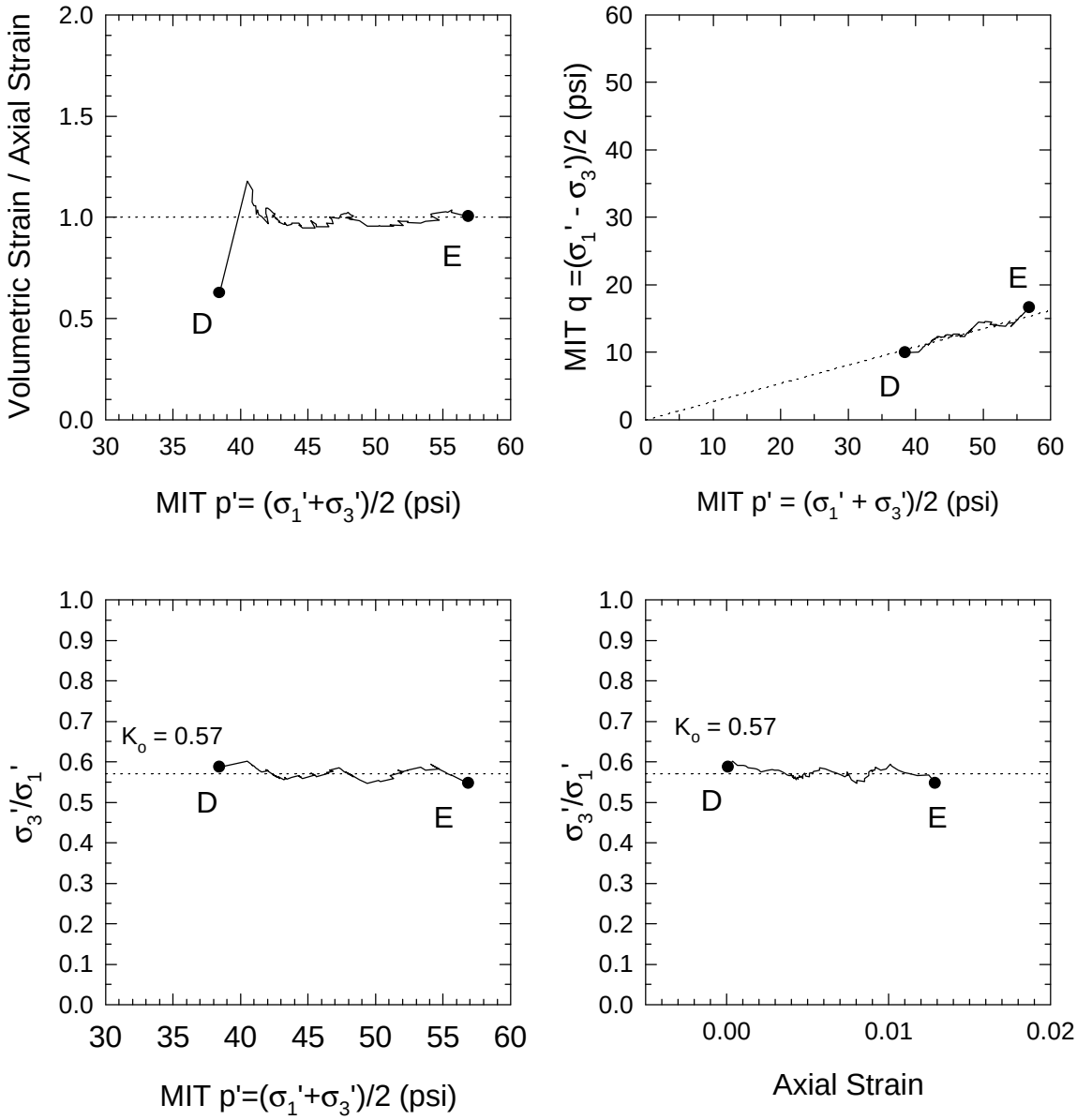

Figure 3.23 K_o Consolidation Test Ko_2 on SB1

Test CU_15 on SB1
σ'_{1con}=73.52 psi, σ'_{3con}=40.21psi
K_o Consolidated as Ko_2 and Sheared at OCR=1.00 as CU_15

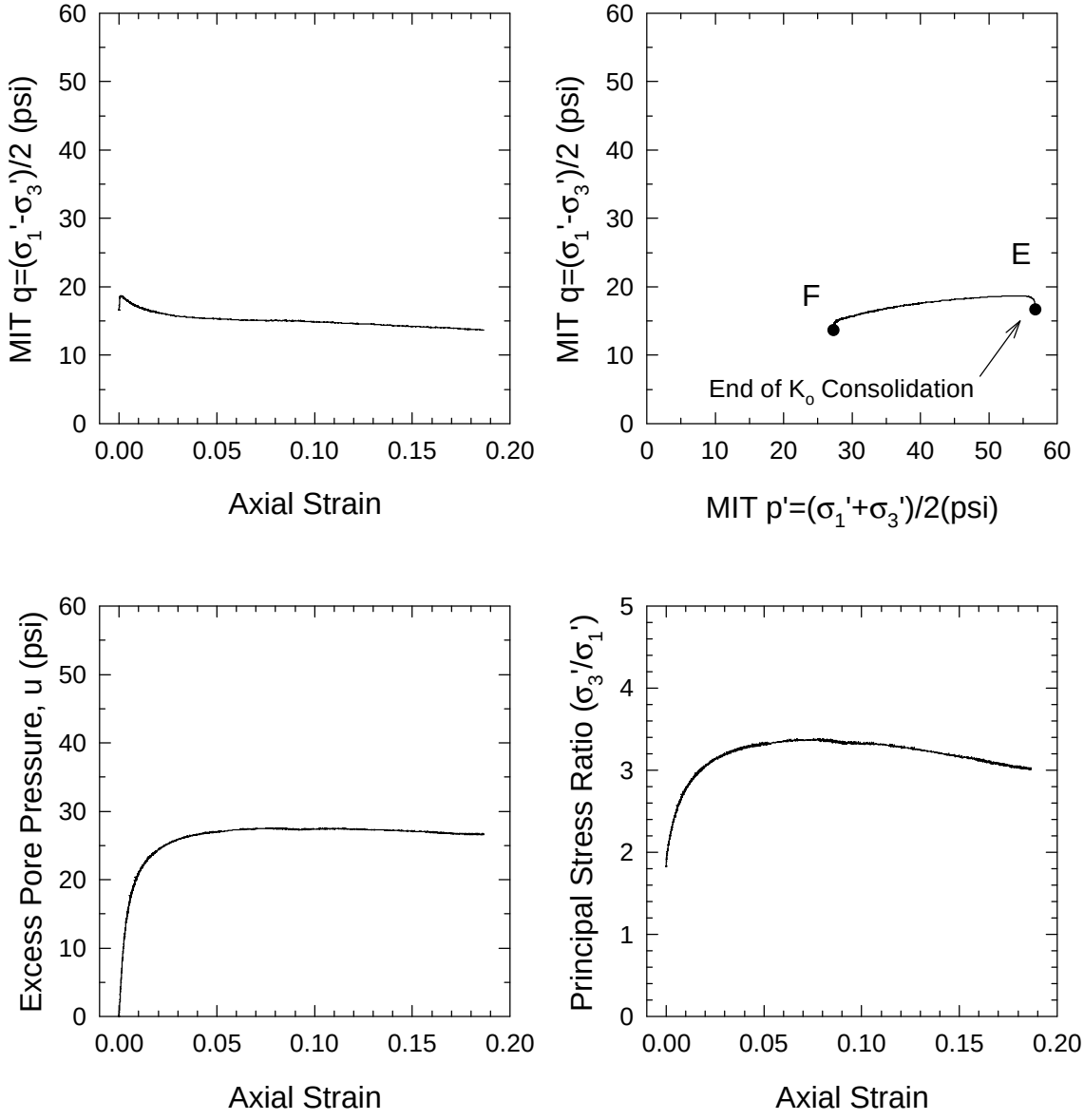

Figure 3.24 K_o Consolidated Undrained Triaxial Test CU_15 on SB1

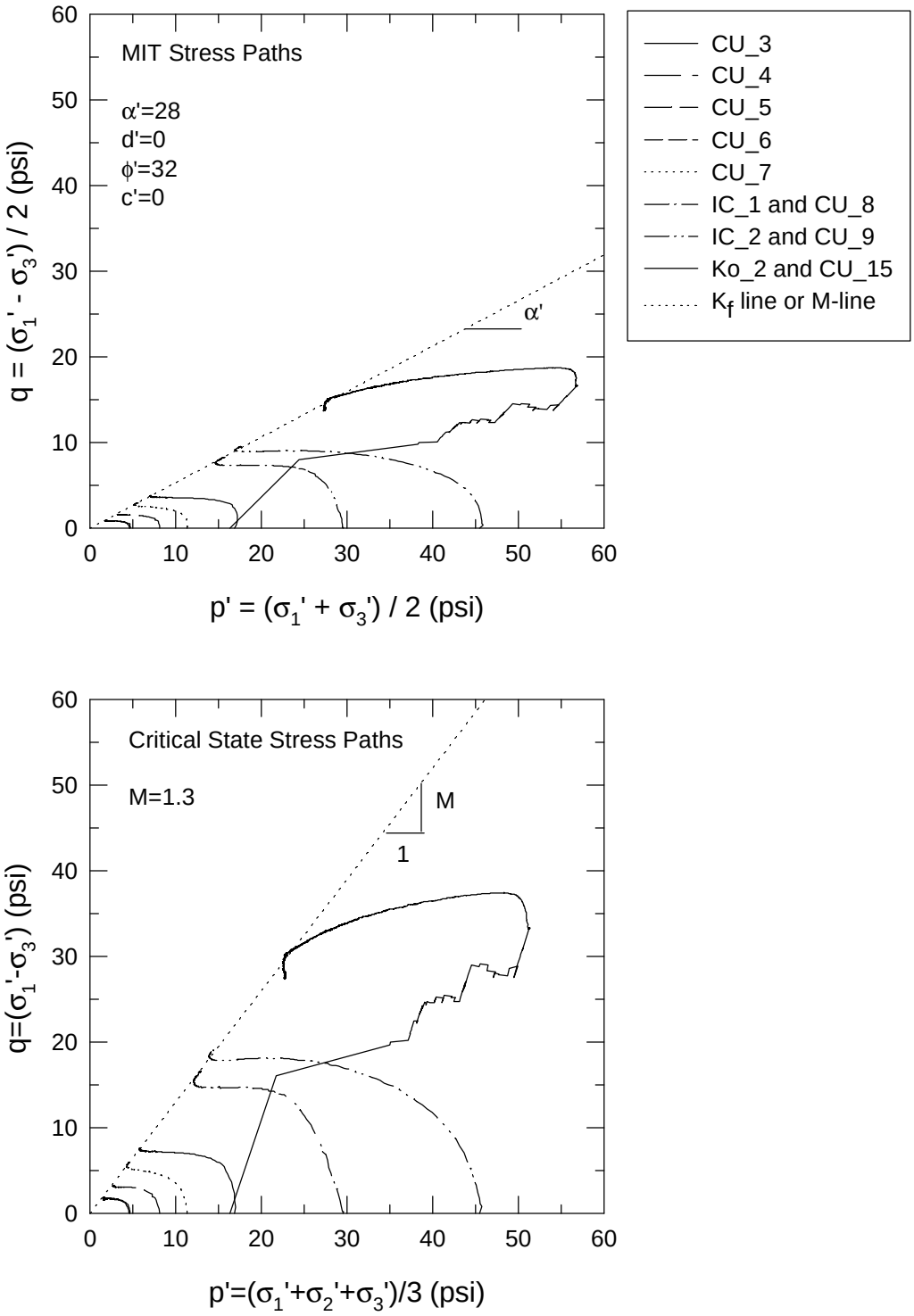

Figure 3.25 Undrained Strength Envelope for SB1

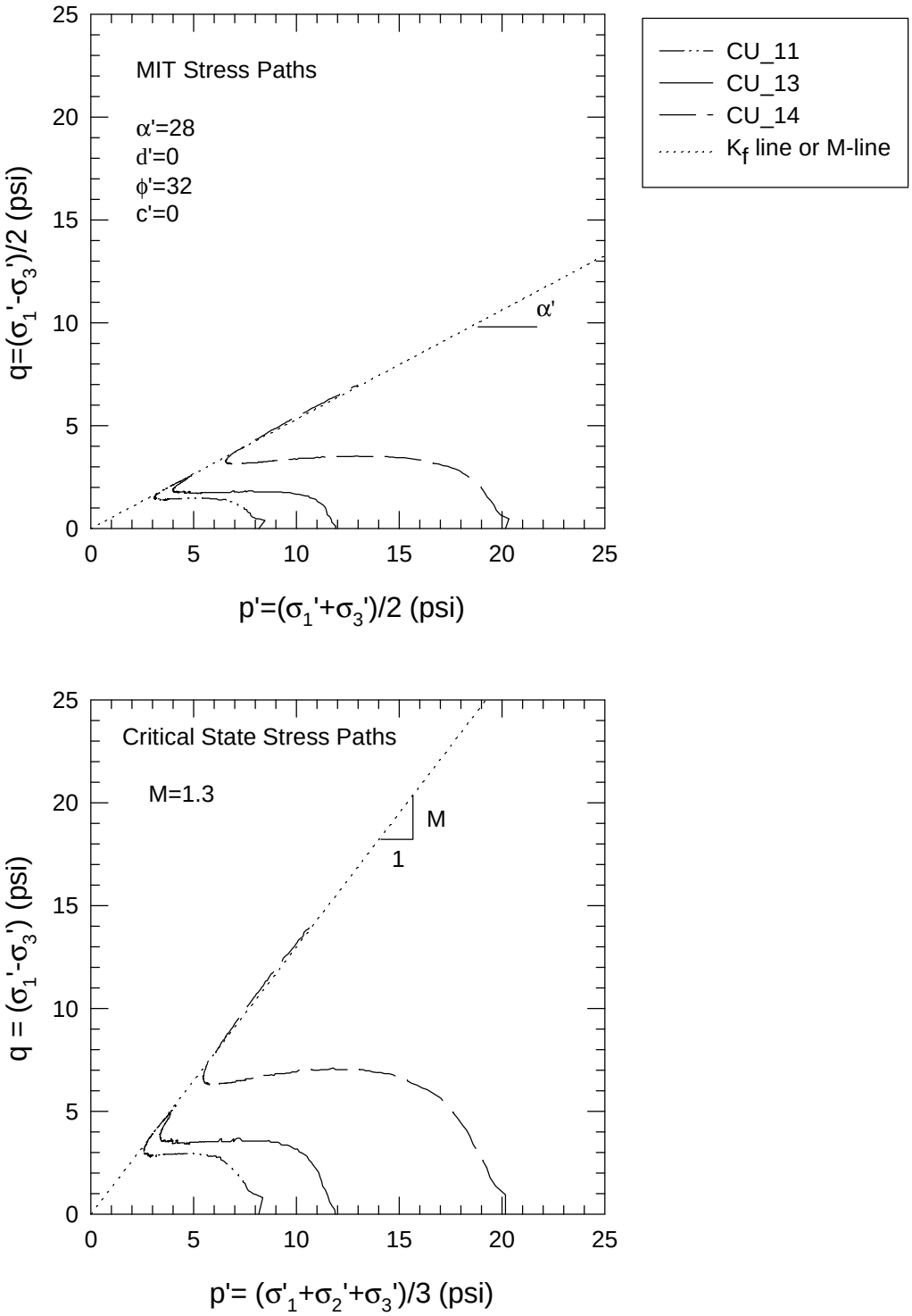

Figure 3.26 Undrained Strength Envelope for SB3

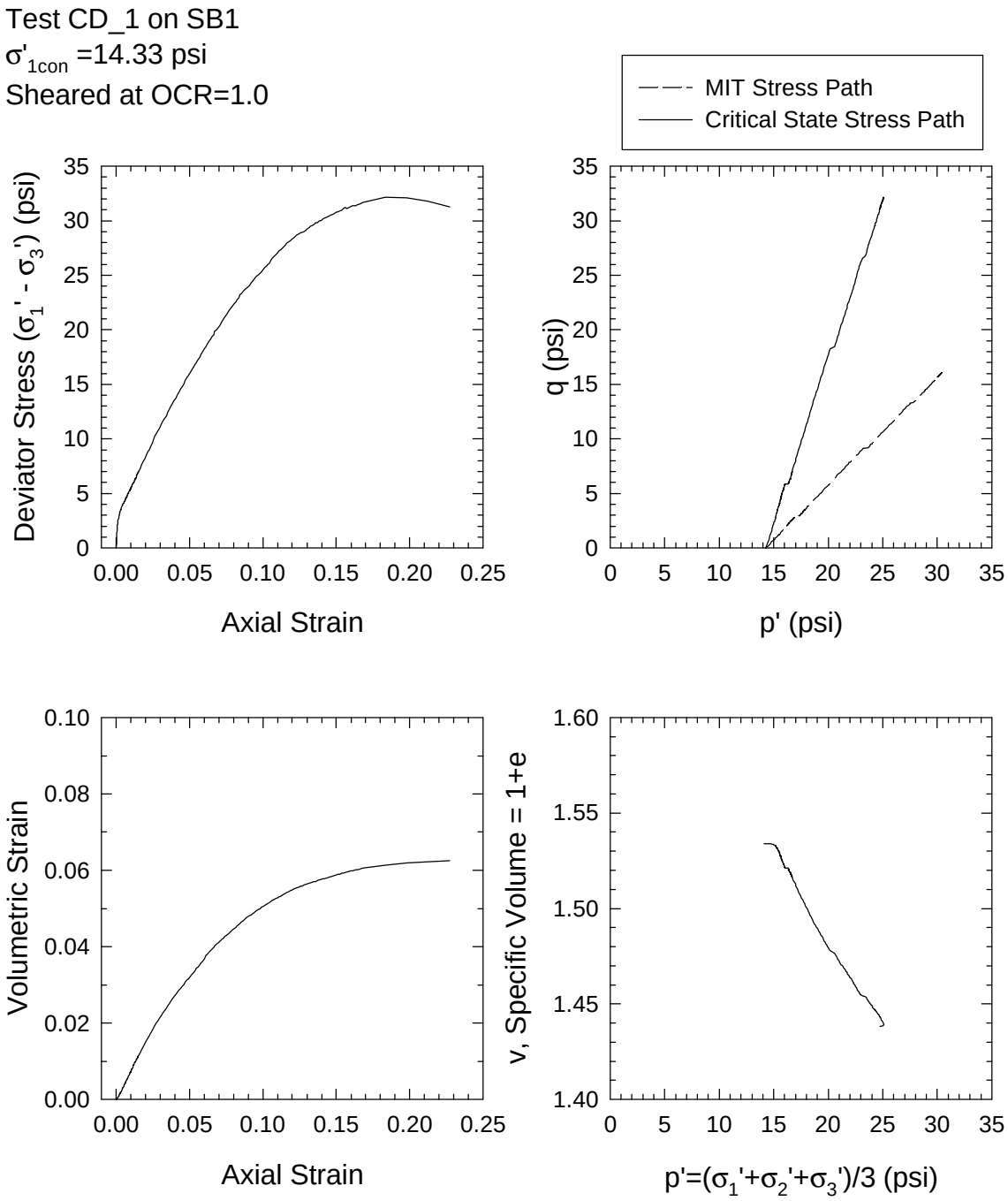

Figure 3.27 Consolidated Drained Triaxial Test CD_1 on SB1

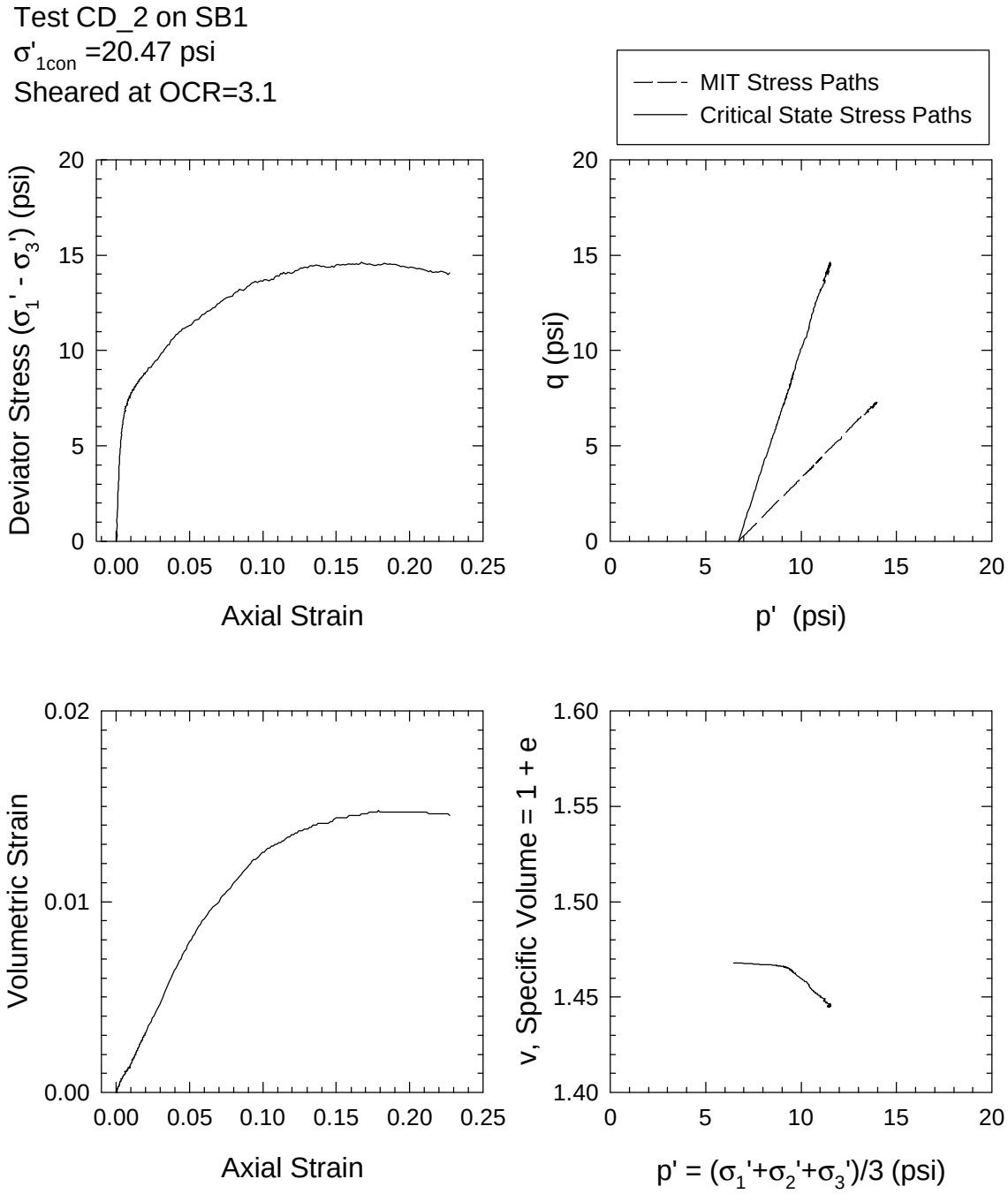

Figure 3.28 Consolidated Drained Triaxial Test CD_2 on SB1

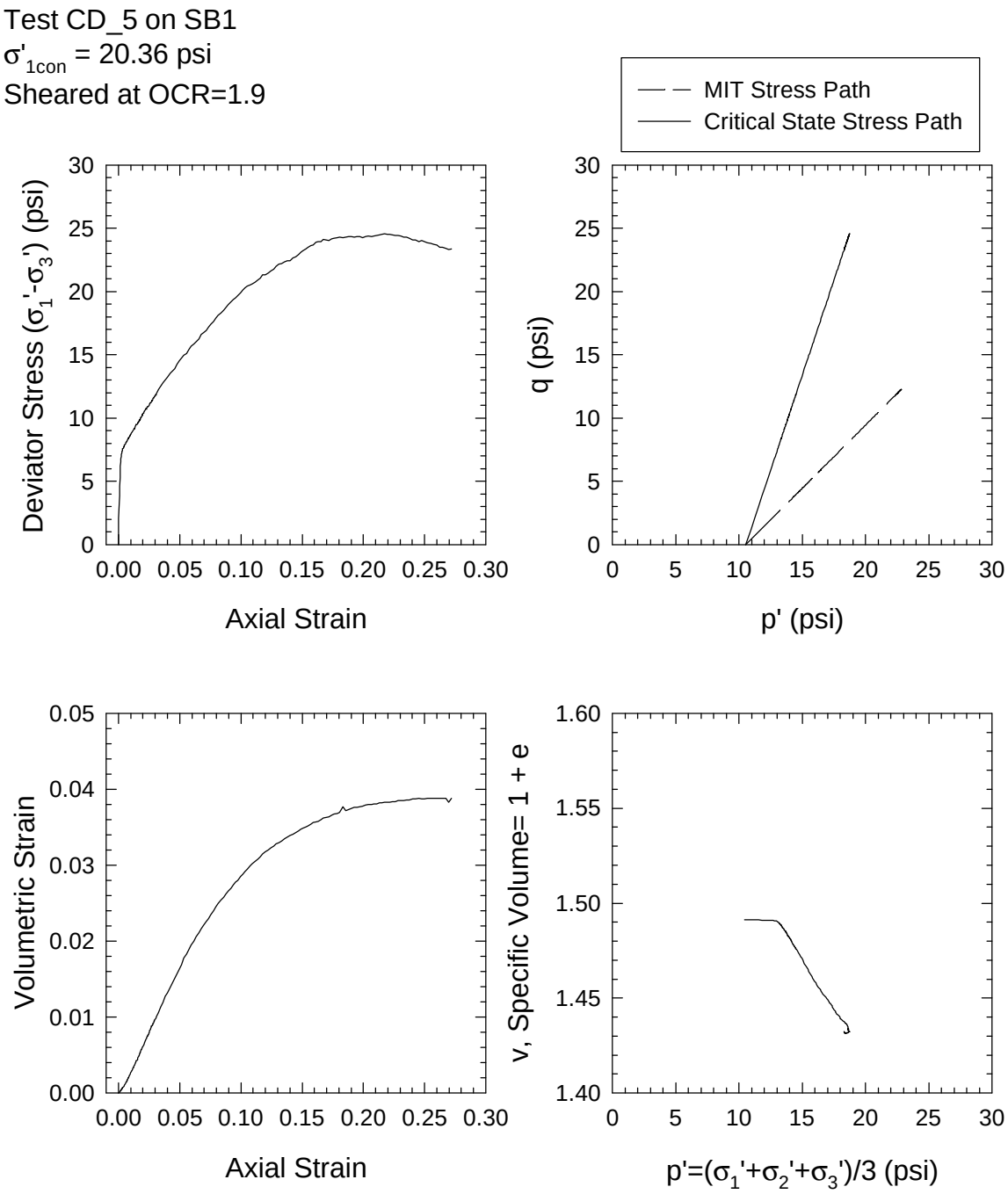

Figure 3.29 Consolidated Drained Triaxial Test CD_5 on SB1

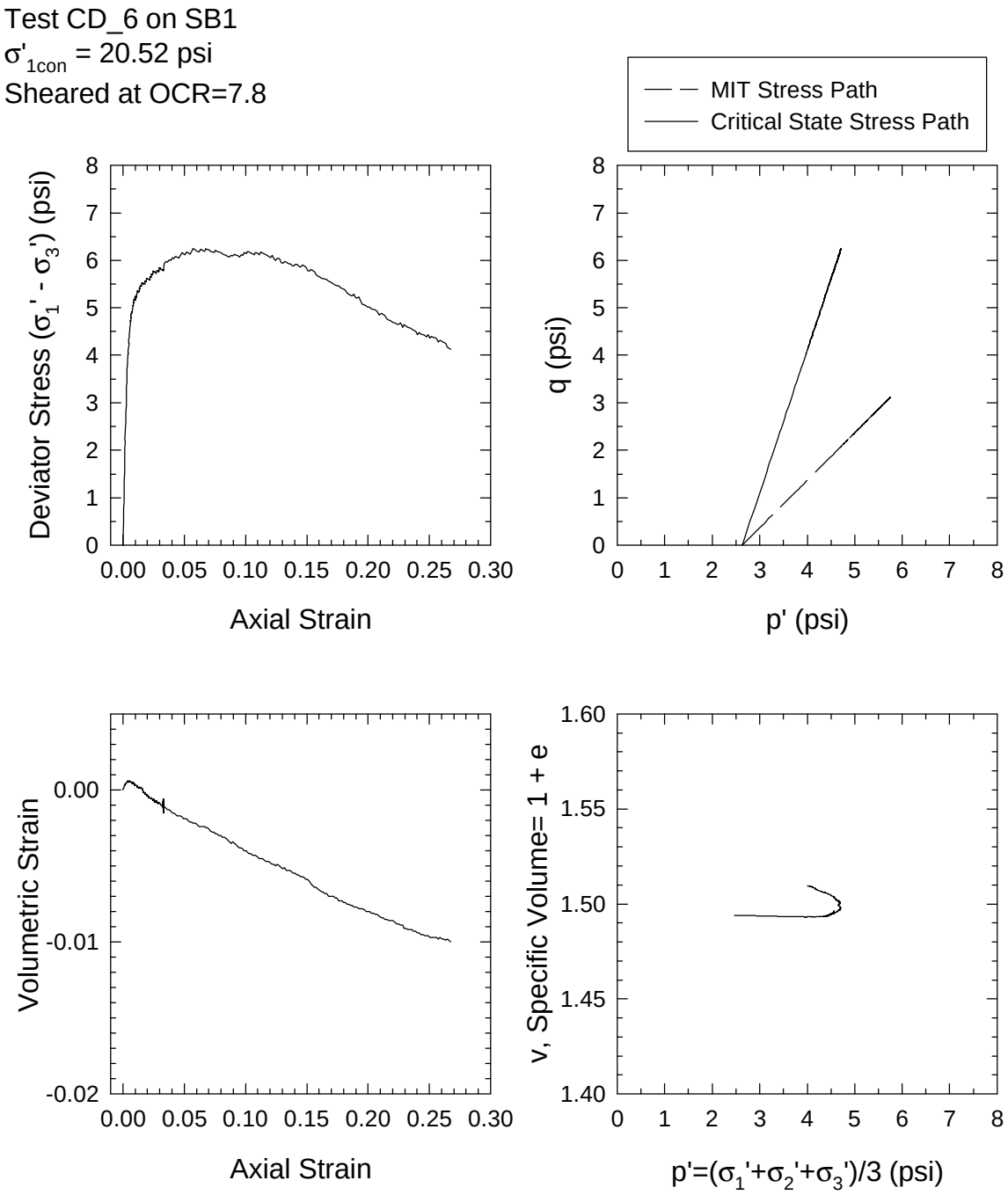

Figure 3.30 Consolidated Drained Triaxial Test CD_6 on SB1

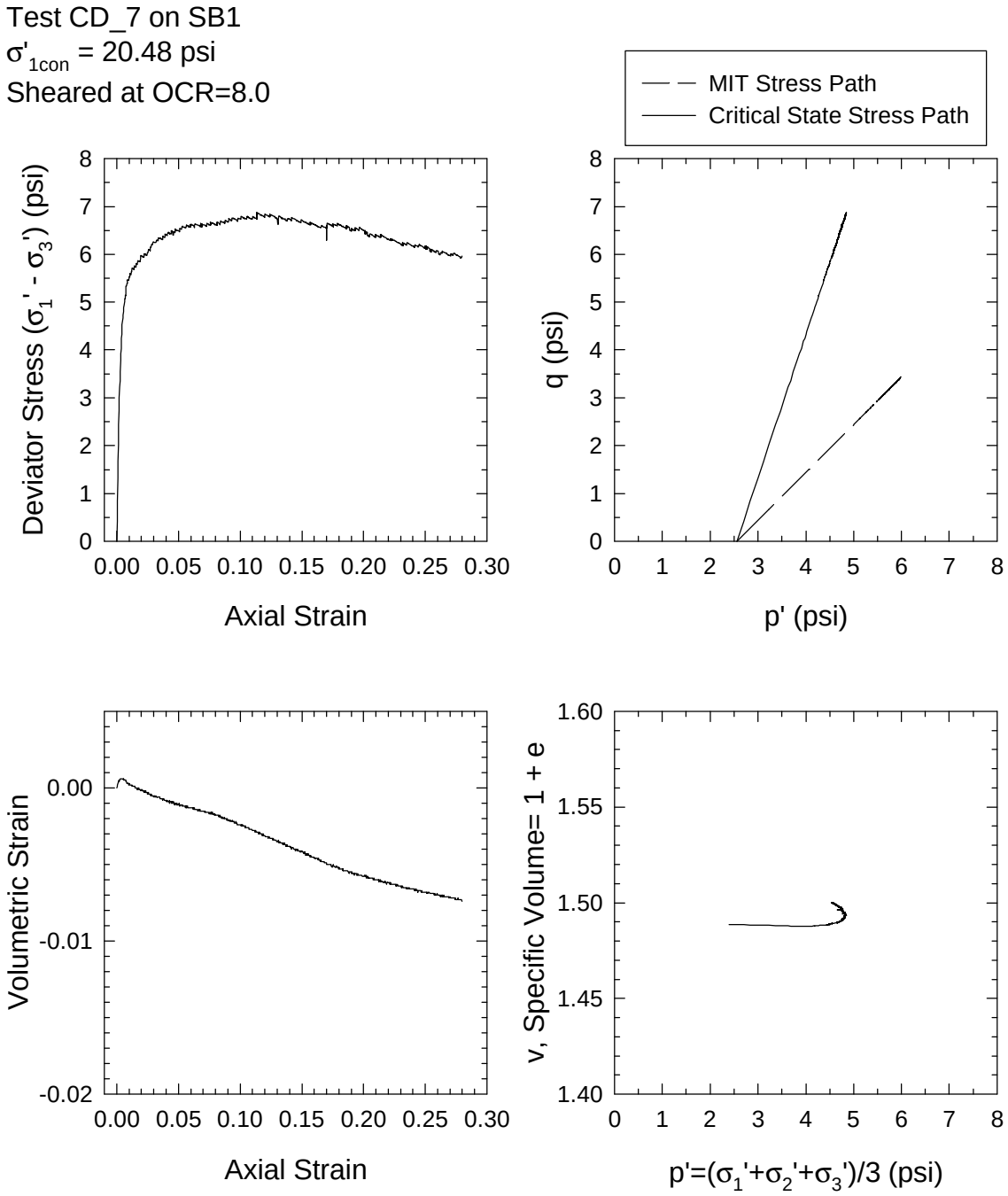

Figure 3.31 Consolidated Drained Triaxial Test CD_7 on SB1

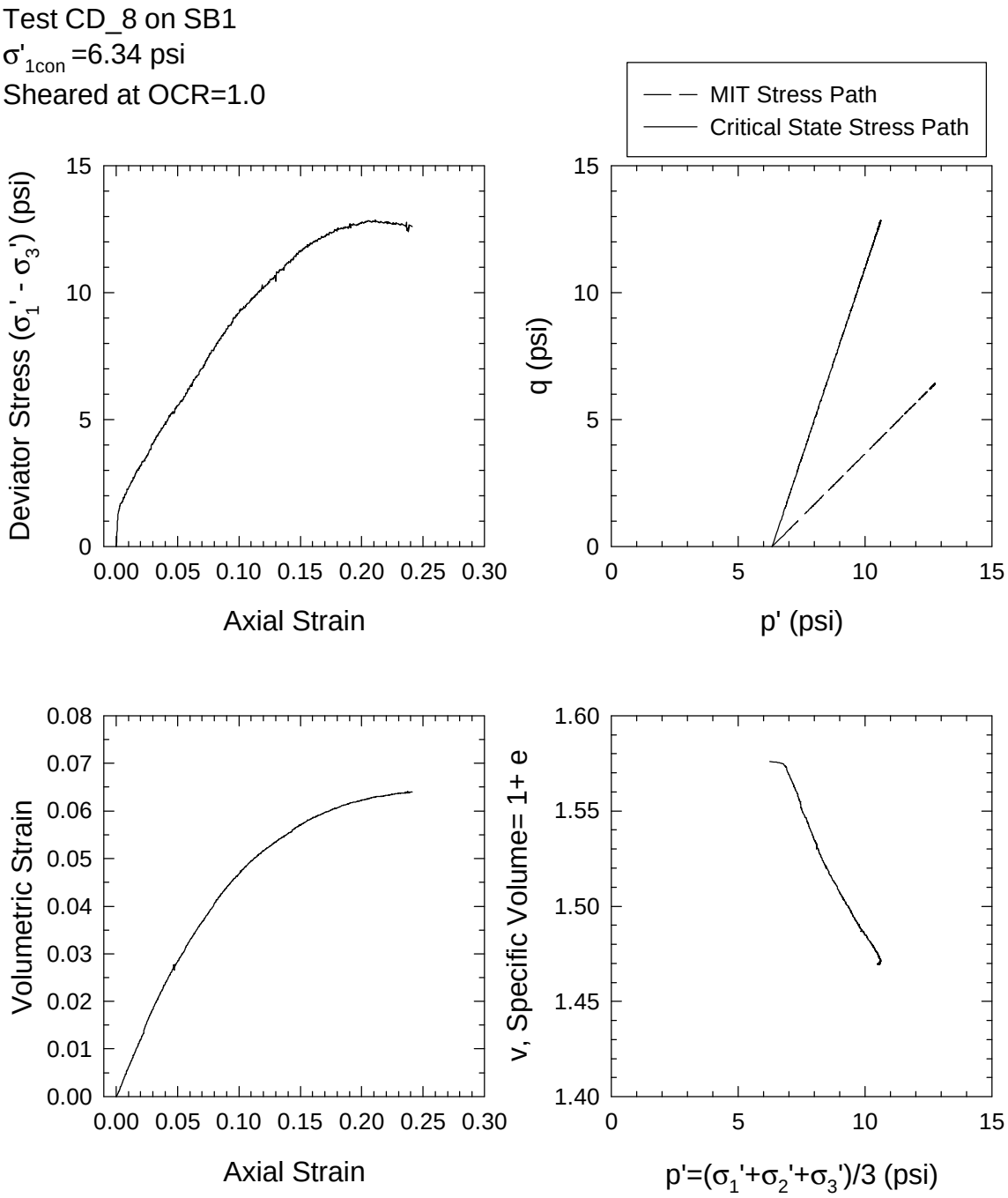

Figure 3.32 Consolidated Drained Triaxial Test CD_8 on SB1

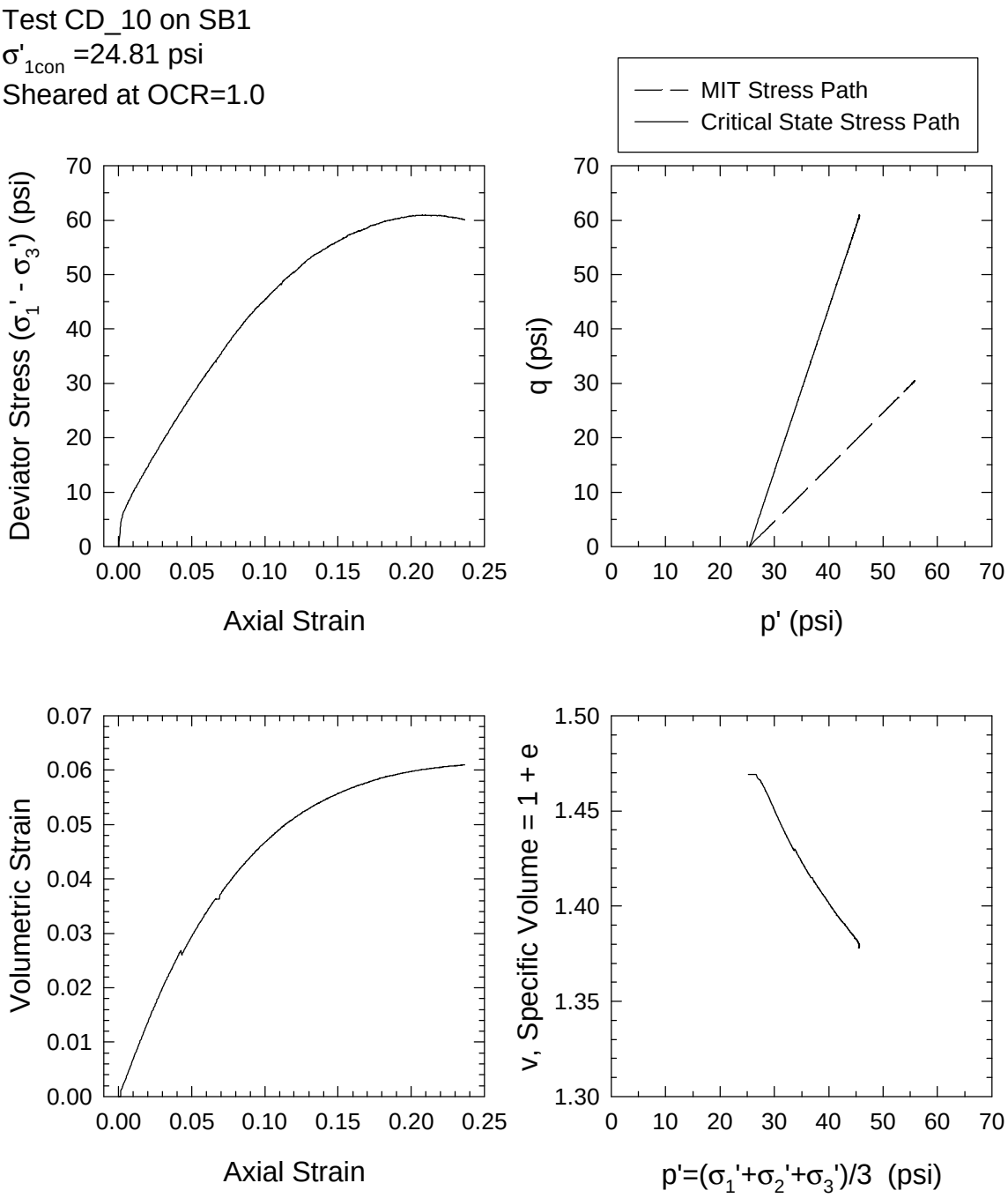

Figure 3.33 Consolidated Drained Triaxial Test CD_10 on SB1

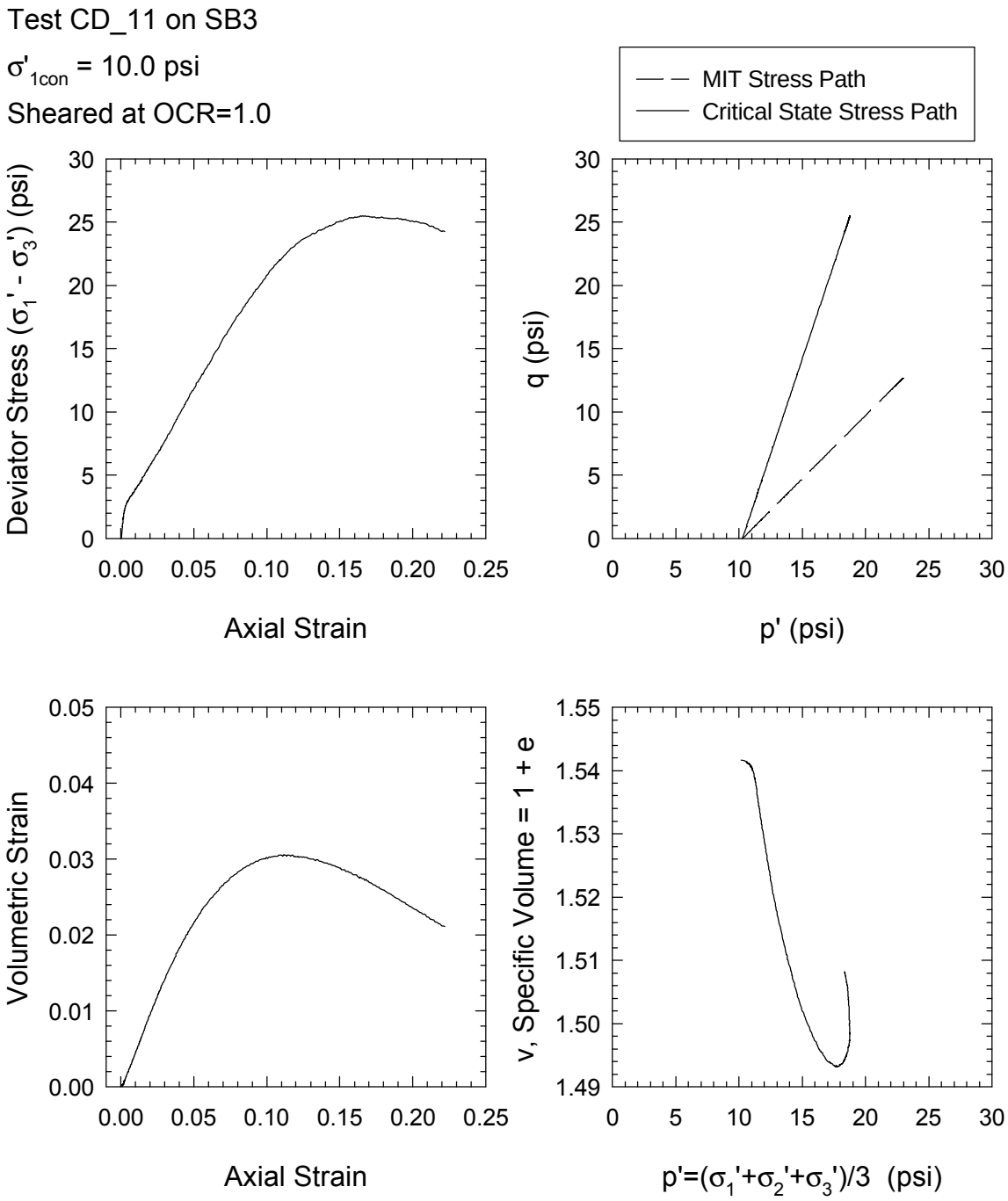

Figure 3.34 Consolidated Drained Triaxial Test CD_11 on SB3

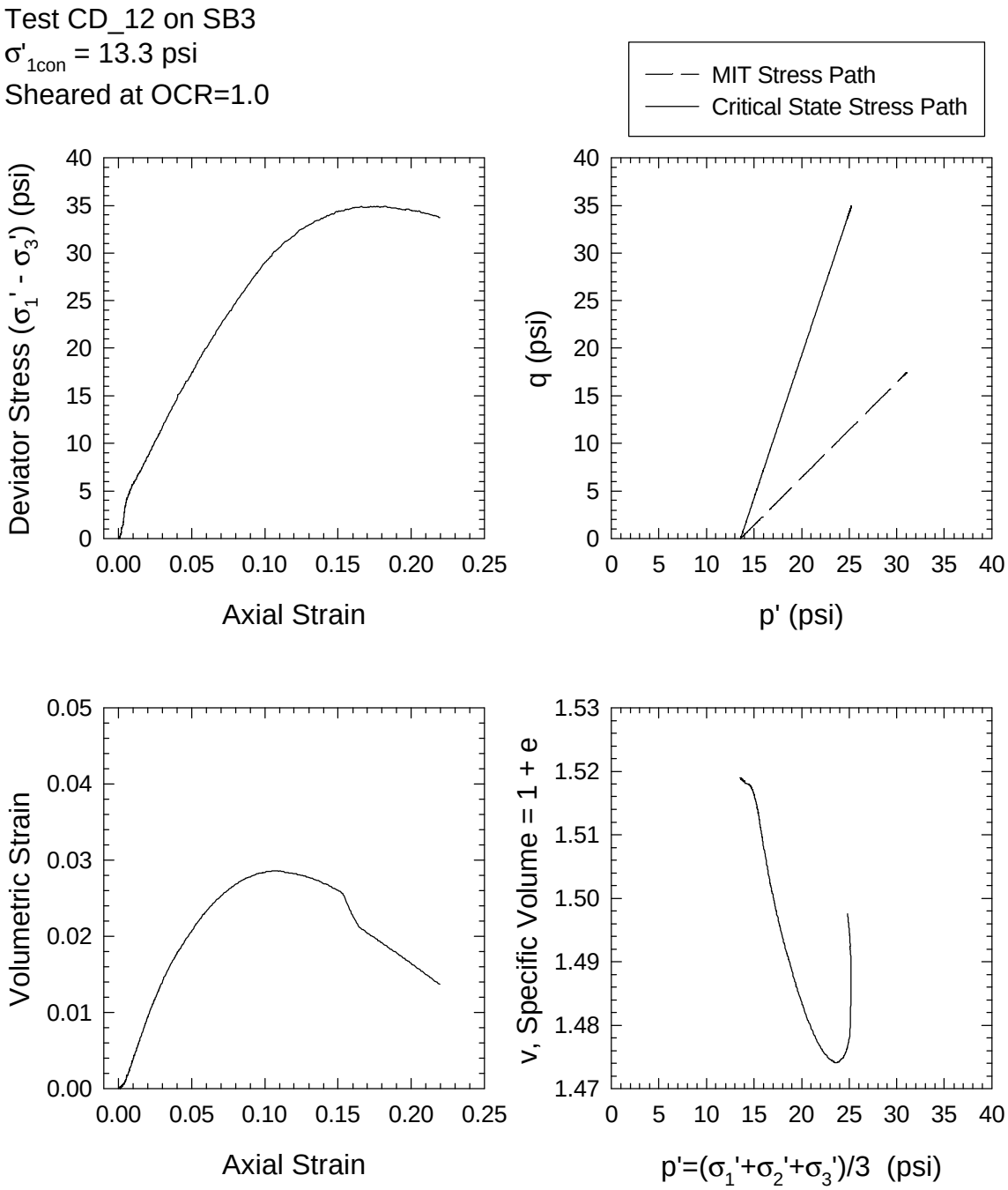

Figure 3.35 Consolidated Drained Triaxial Test CD_12 on SB3

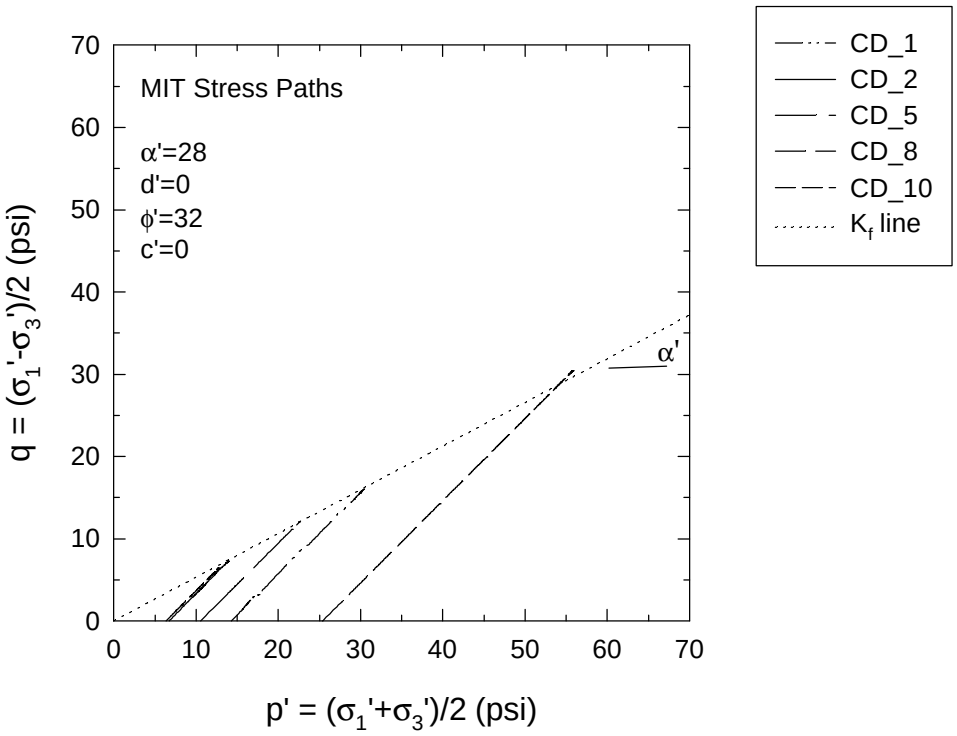

Figure 3.36 Drained Strength Envelope for SB1

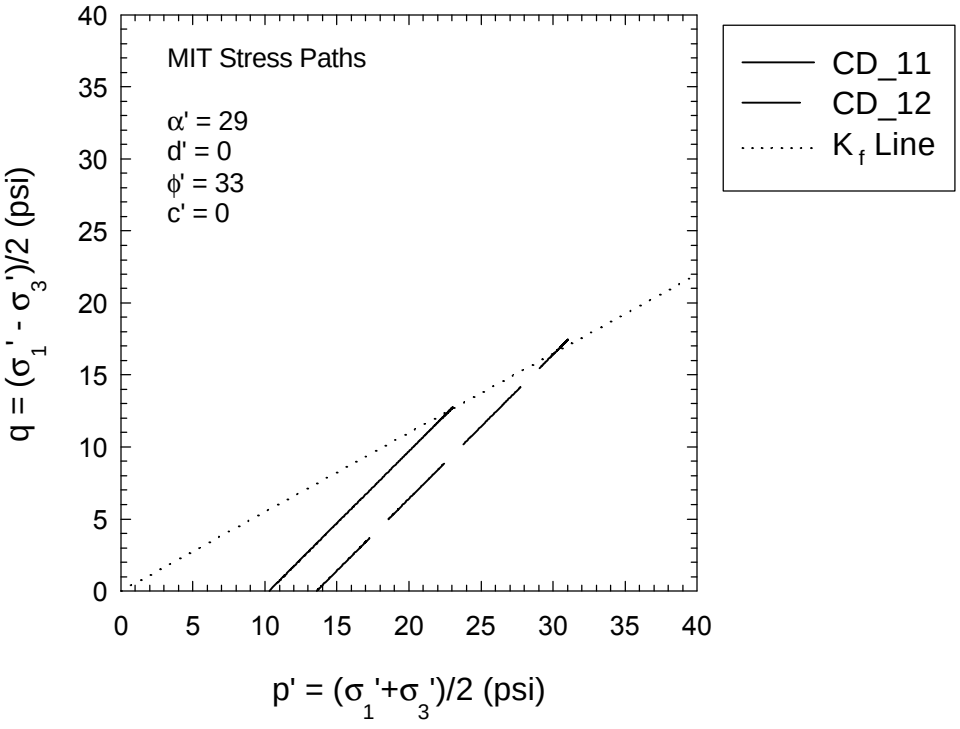

Figure 3.37 Drained Strength Envelope for SB3